## General Disclaimer

## One or more of the Following Statements may affect this Document

- This document has been reproduced from the best copy furnished by the organizational source. It is being released in the interest of making available as much information as possible.

- This document may contain data, which exceeds the sheet parameters. It was furnished in this condition by the organizational source and is the best copy available.

- This document may contain tone-on-tone or color graphs, charts and/or pictures, which have been reproduced in black and white.

- This document is paginated as submitted by the original source.

- Portions of this document are not fully legible due to the historical nature of some of the material. However, it is the best reproduction available from the original submission.

GENERAL ELECTRIC

SCHENECTADY, NEW YORK

FINAL REPORT

# DESIGN, DEVELOPMENT, FABRICATION, AND DELIVERY OF FLUIDIC ACCELEROMETERS

Prepared for

George C. Marshall Space Flight Center
Astrionics Laboratory
NASA, Huntsville, Alabama



Contract No. NAS 8-20729



March 28, 1968

# FINAL REPORT

# DESIGN, DEVELOPMENT, FABRICATION AND DELIVERY OF FLUIDIC ACCELEROMETERS

Prepared for:

George C. Marshall Space Flight Center
Astrionics Laboratory
NASA, Huntsville, Alabama

Contract No.

NAS 8-20729

Prepared by:

General Electric Company
Specialty Fluidics Operation
Schenectady, New York

TABLE OF CONTENTS

## LIST OF FIGURES

## NOMENCLATURE

$A_N$ - Nozzle Area

$a_i$ - Applied Acceleration

D - Displacement of Jet Pipe

$D_o$ - Initial misalignment of Jet Pipe

$D_{max}$ - Maximum displacement of Jet Pipe

E - Modules of elasticity

F - Applied Force

$F_o$ - Output Force

$f_o$ - Resonant frequency in HZ

G - Proportional Gain

$G_B$ - Blocked load Amplifier Gain

$G_o$ - Reset Gain

g - Operational Constant

$g_r$ - g range

$g_a$ - Applied g

I - Cross sectional moment of Inertia

k - Ratio of ID to wall thickness

$K_f$ - Flexure Gradient

| | | |
|---|---|---|
| $K_n$ | - | Nozzle Force Coefficient |
| L | - | Inductance |
| l | - | Length |
| $\Delta P_o$ | - | Accelerometer Output Pressure |
| $\Delta P_B$ | - | Open loop Bias Pressure |
| $\Delta P_f$ | - | Closed loop Bias Pressure |
| $R_o$ | - | Amplifier Output Impedance |
| $R_i$ | - | Input Impedance |
| $R_f$ | - | Feedback Resistance |
| $R_s$ | - | Tube Resistance |
| S | - | La place Operator |
| T | - | Time Constant |
| $\delta$ | - | Damping Factor |
| $W_n$ | - | Flexure Resonance rad/sec |
| $w_o$ | - | System Cross over rad/sec |
| W | - | Weight of Seismic Mass |

## 1.0 INTRODUCTION

This report gives the results of work done on contract NAS 8-20729 "Design, Development, Fabrication and Delivery of Fluidic Accelerometers." The contract was supported by the George C. Marshall Space Flight Center, Astrionics Laboratory, NASA, Huntsville Alabama.

Two fluidic accelerometers were designed, developed and tested on this contract. The accelerometers are of the closed loop force balance type with a differential output pressure directly proportional to acceleration.

## 2.0 SUMMARY

### 2.1 Design Goals

Two fluidic accelerometers were developed using the following specifications as design goals.

Range- ± 1g

Fluid Media- Air filtered to 25 microns

Supply Pressure- 20 psig. The device will have structural capability of operating at 100 psig.

Maximum output Pressure- The output pressure for an input of 1g will be at least 5 psig with a supply pressure of 20 psig. The maximum flow rate will be .1 scfm or greater.

Linearity- The output will be within the limits described in Figure 2.1.

Temperature Operating Range- From $0^{\circ}$ to $350^{\circ}$F.

Frequency Response- Within the specified region as described in Figure 2.2.

Acceptable Phase Lag- The phase angle will be equal to or less than the phase lag of a linear second order system with a natural frequency of 80 cps and peaking of 1 db or greater.

### 2.2 System and Hardware Description

A schematic of the fluidic accelerometer is shown in Figure 2.3. The basic sensor is a seismic mass M supported by a soft flexure P. The flexure has a hollow tube to produce a jet impinging on two fluidic receivers A.

Acceleration of the mass along the sensitive axis results in a displacement of the mass and jet pipe relative to the pick-off probe. The resulting differential signal pressure is amplified and applied to the nulling nozzles N, to produce a force to restore the mass to its neutral position. Closed loop operation maintains the restoring force (proportional to the differential pressure $\Delta P_o$) equal to the force accelerating the mass. The scale factor (Psi per g) is then a function of the mass and of the area of the nulling nozzles.

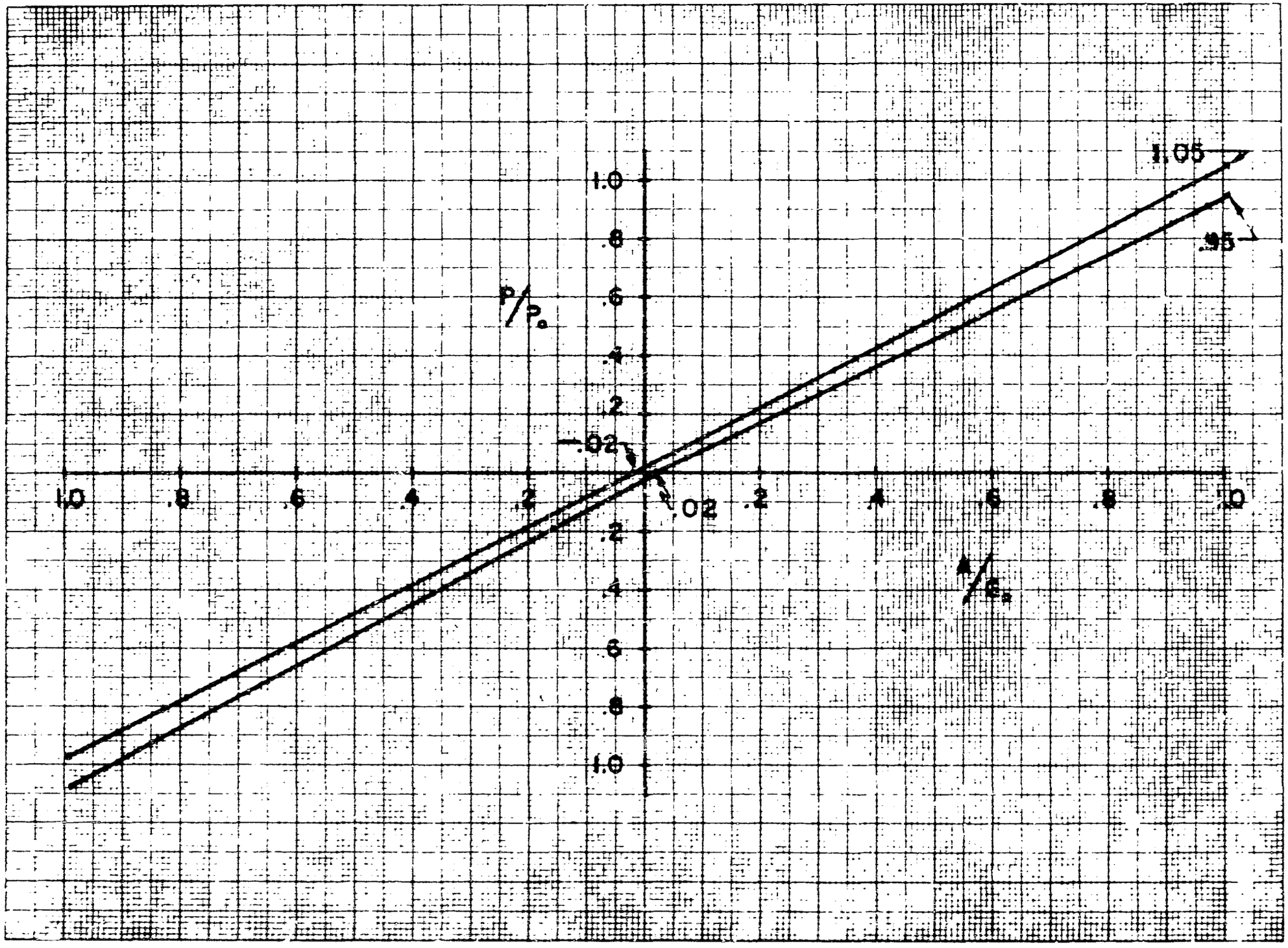


FIG. 2.1 LINEARITY REQUIREMENTS

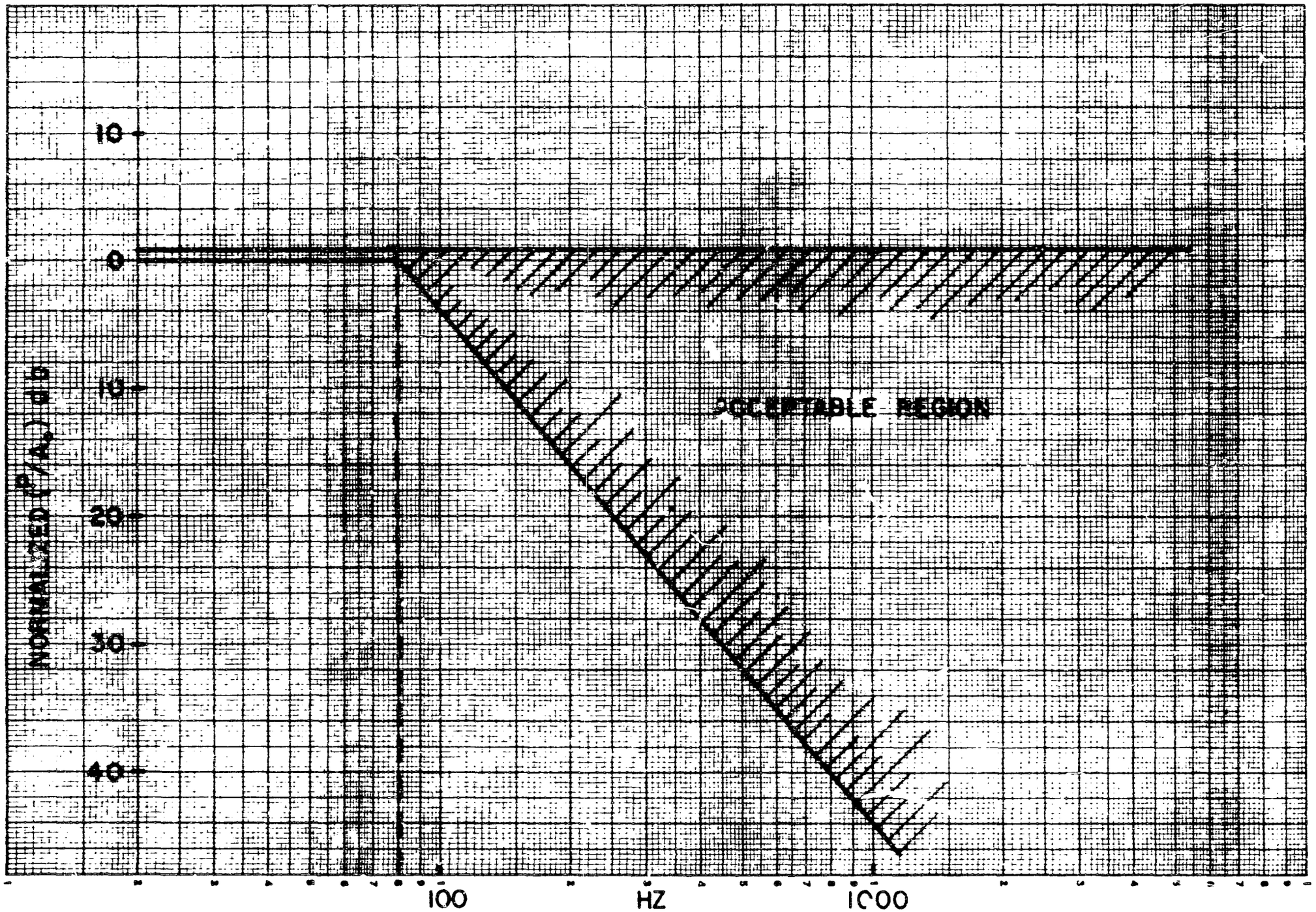


FIG. 2.2 RESPONSE REQUIREMENTS

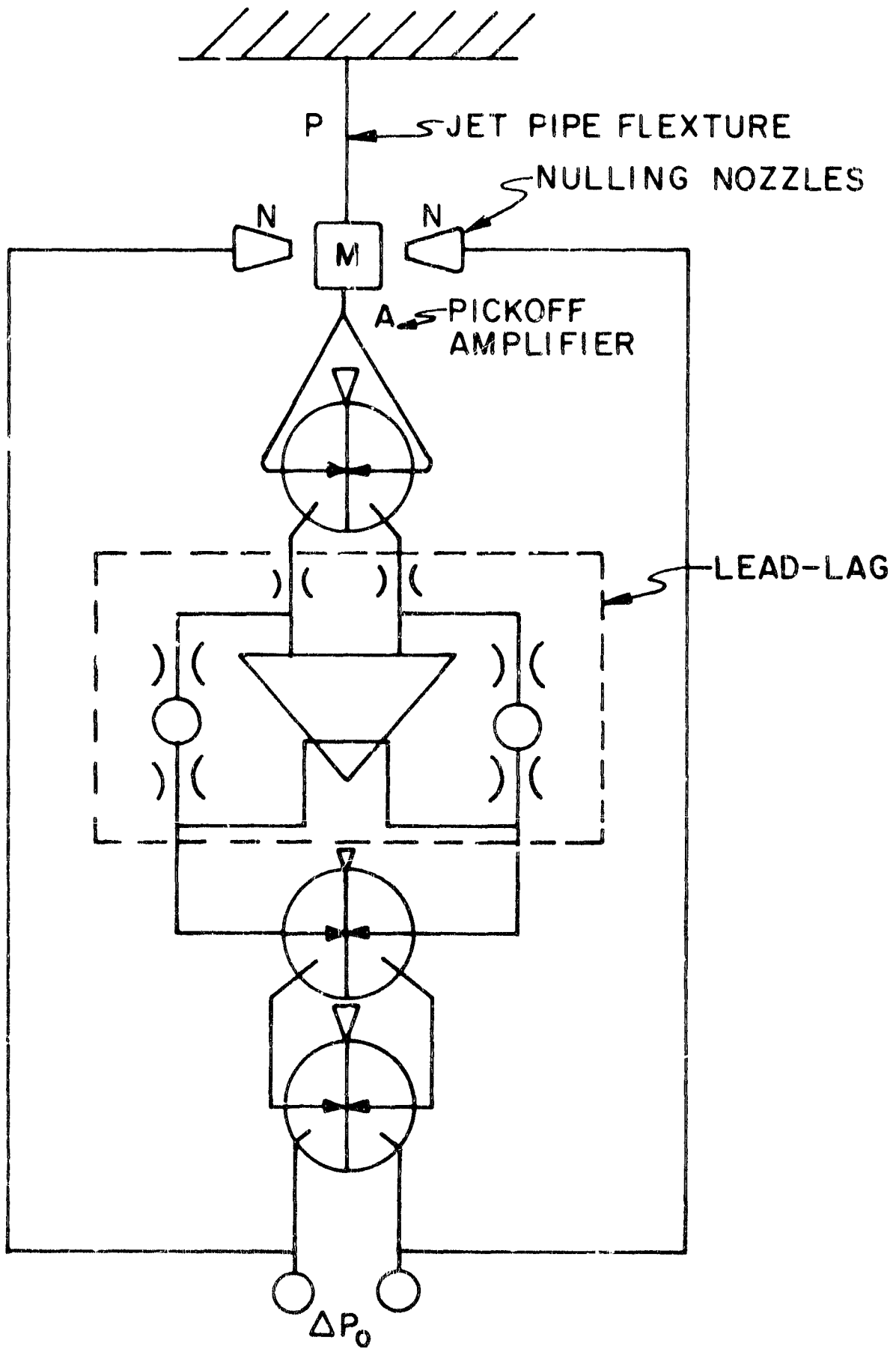


FIG. 2.3 – ACCELEROMETER SCHEMATIC

The spring-mass system comprised of the seismic mass and flexure has very low inherent damping and will be oscillatory unless additional damping is provided. The additional damping required is provided by a fluidic lead-lag circuit.

The principal advantages of this approach are:

- No close fitting sliding parts are used.
- The output signal is essentially independent of supply pressure and gain variations.
- Characteristics such as response, range and scale factor can be conveniently varied by adjustments in the feedback amplifier. For example, the scale factor can be varied by changing the nulling nozzle area.

Figures 2.4 and 2.5 are photographs of the hardware delivered on this program. Figure 2.4 shows the assembled accelerometer. All the component parts such as the seismic mass, pick-off amplifier, lead-lag circuit and power amplifier are mounted on a rigid base which also serves as a manifold for interconnecting amplifiers and distributing of supply pressure to the amplifiers. The component parts are mounted to make the signal path as short as possible. The overall response of the accelerometer is highly dependent on this path length. In Figure 2.5 the nulling nozzle assembly and the pick-off amplifier have been removed to show the seismic mass and flexure. All the component parts of the flexure assembly - base, flexure and seismic mass - are stainless steel joined by soldering. The center flexure member is a hollow tube with an inner diameter of .01 inches and also functions as the jet pipe for the pick-off amplifier. Two additional wires are used to stiffen the flexure along the insensitive axis. The pick-off amplifier is provided with a mechanical stop which restricts movement of the jet pipe to the linear range of the pick-off amplifier. Vernier nulling of the accelerometer is done by positioning the pick-off amplifier along the sensitive axis so that the differential output of the nulling nozzles is zero when zero acceleration is applied along the sensitive axis. The output of the pick-off amplifier ccuples directly into the lead-lag circuit mounted on the vertical face of the manifold. The cylindri-

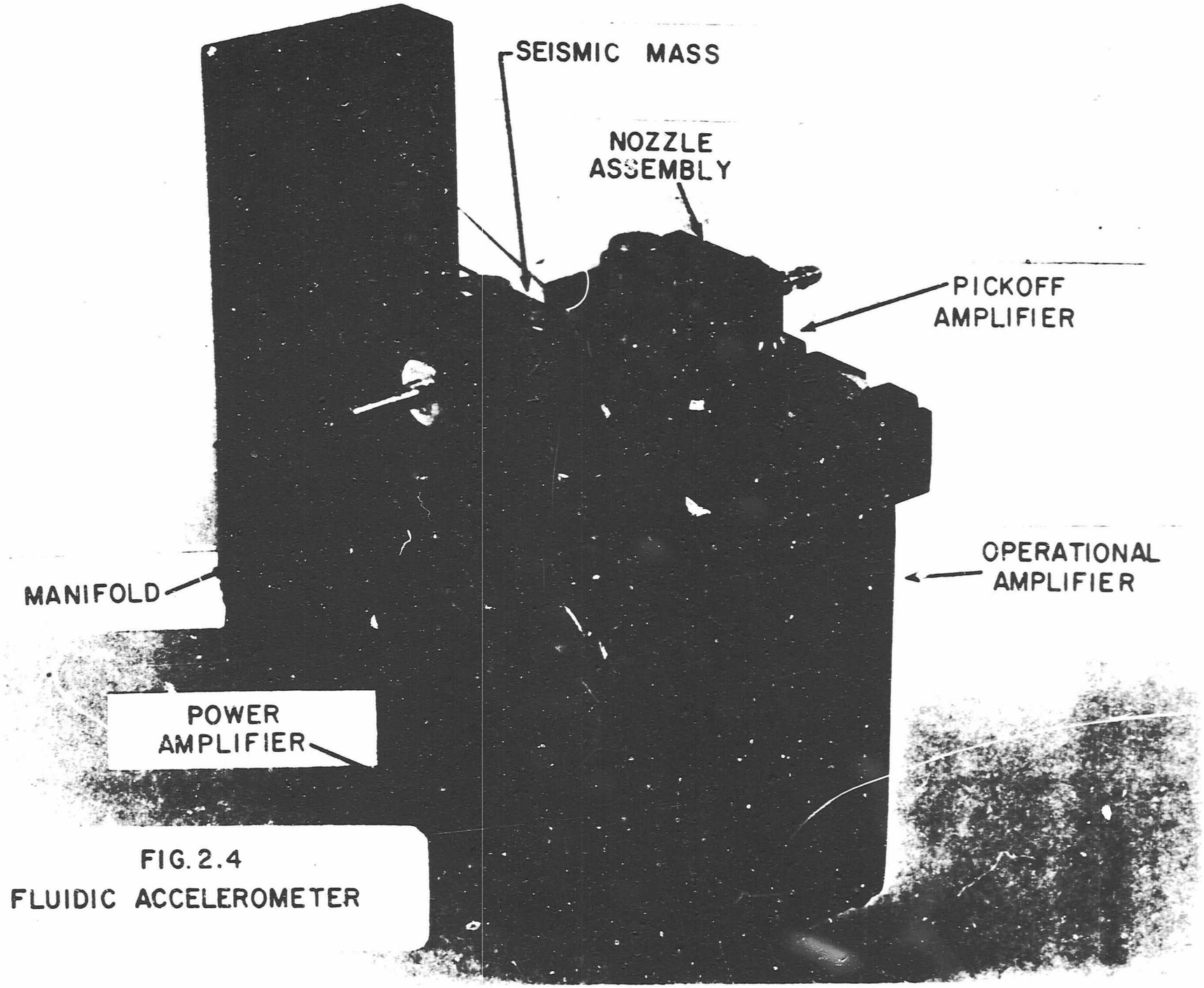


FIG. 2.4
FLUIDIC ACCELEROMETER

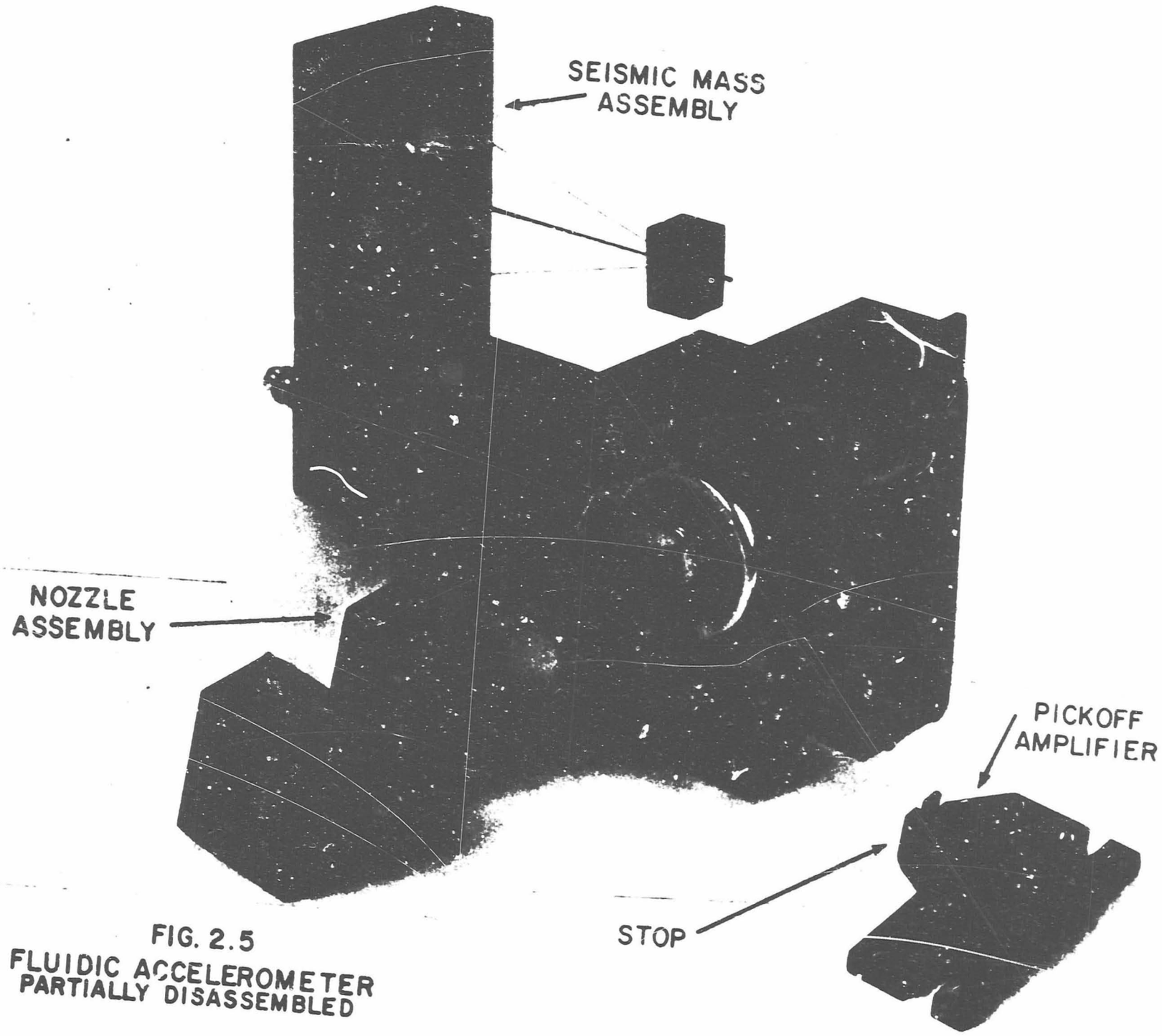


FIG. 2.5
FLUIDIC ACCELEROMETER
PARTIALLY DISASSEMBLED

cal can on either side of the manifold is a fluid capacity used in the feedback of the operational amplifier. The output of the operational amplifier couples directly to the two stage output amplifier mounted on the bottom surface of the manifold. A channel through the manifold block couples the output amplifier to the nozzle block. The output of the accelerometer is taken off either side of the nozzle block.

## 2.3 Test Results Summary

The hardware delivered on this program deviated from the original design goals as follows:

1. The range on the accelerometer is ± .8g as compared to the design goal of ± 1g. The range is strongly dependent on circuit bandwidth in this configuration.

The ± .8 max g limitation results from a bandwidth limitation rather than a force limitation. The max. range can be made relatively independent of bandwidth by incorporating an integrator in the fluidic circuit. A complete redesign of the manifold and base would be required to incorporate the integrator. This modification is recommended for all applications requiring a range in excess of ± .5g.

2. Frequency response falls outside the specified region in several frequency bands. The measured response is superimposed on the design goals in Figure 2.6. Two sets of measured data are shown; the data exhibiting a 9 db peak at 80 HZ was obtained on an accelerometer with a range of ± .6g. The second set of data was obtained after circuit modification to extend the range to ± .8g. In both cases the peak in the response curve falls outside the acceptable region. This again is a bandwidth limitation and is representative of the "circuit state-of-the-art."

3. The max. temperature operating range is restricted to 300°F as compared to the design goal of 350°F. This restriction is due to the solder used in fabrication of the stainless steel seismic mass and flexure assembly. The accelerometer was tested to +300°F, the scale factor changed less than .5% and null by less than .006g over the range tested. No operational difficulties are

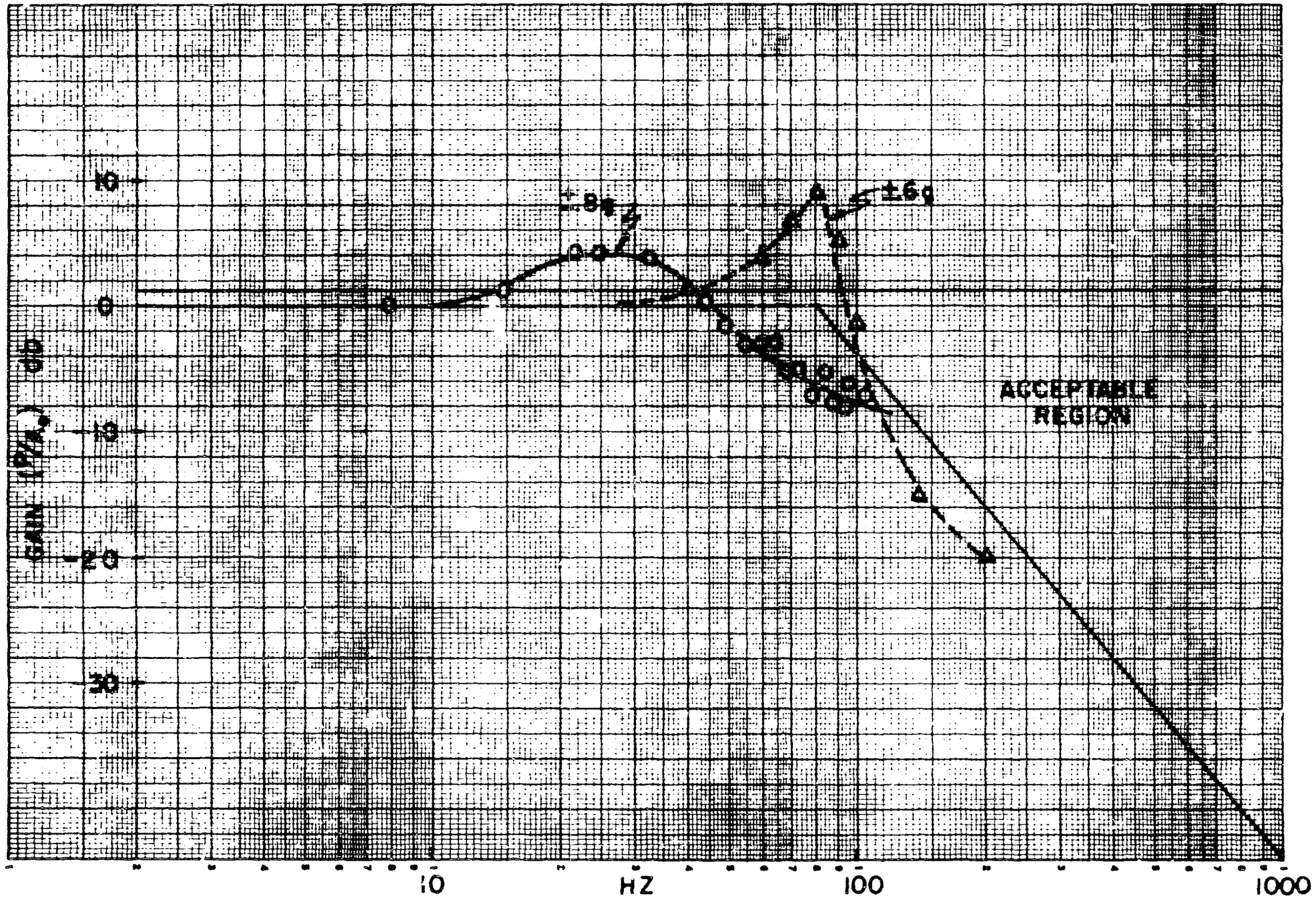


FIG. 2.6 CLOSED LOOP AMPLITUDE DATA

expected at higher temperature ranges. A copper brazed seismic mass assembly will extend the operating temperature to well above the design goal.

Measured closed loop phase lag is compared to the design goal in Figure 2.7 The phase lag on the ± .6g range accelerometer meets the requirements at all frequencies below 80 HZ. Addition of an integrator in the loop will make it possible to meet the phase lag requirements as well as higher ranges of acceleration.

The output vs. g is superimposed on the linearity requirements in Figure 2.8. The output curve falls within the requirements over the complete g range.

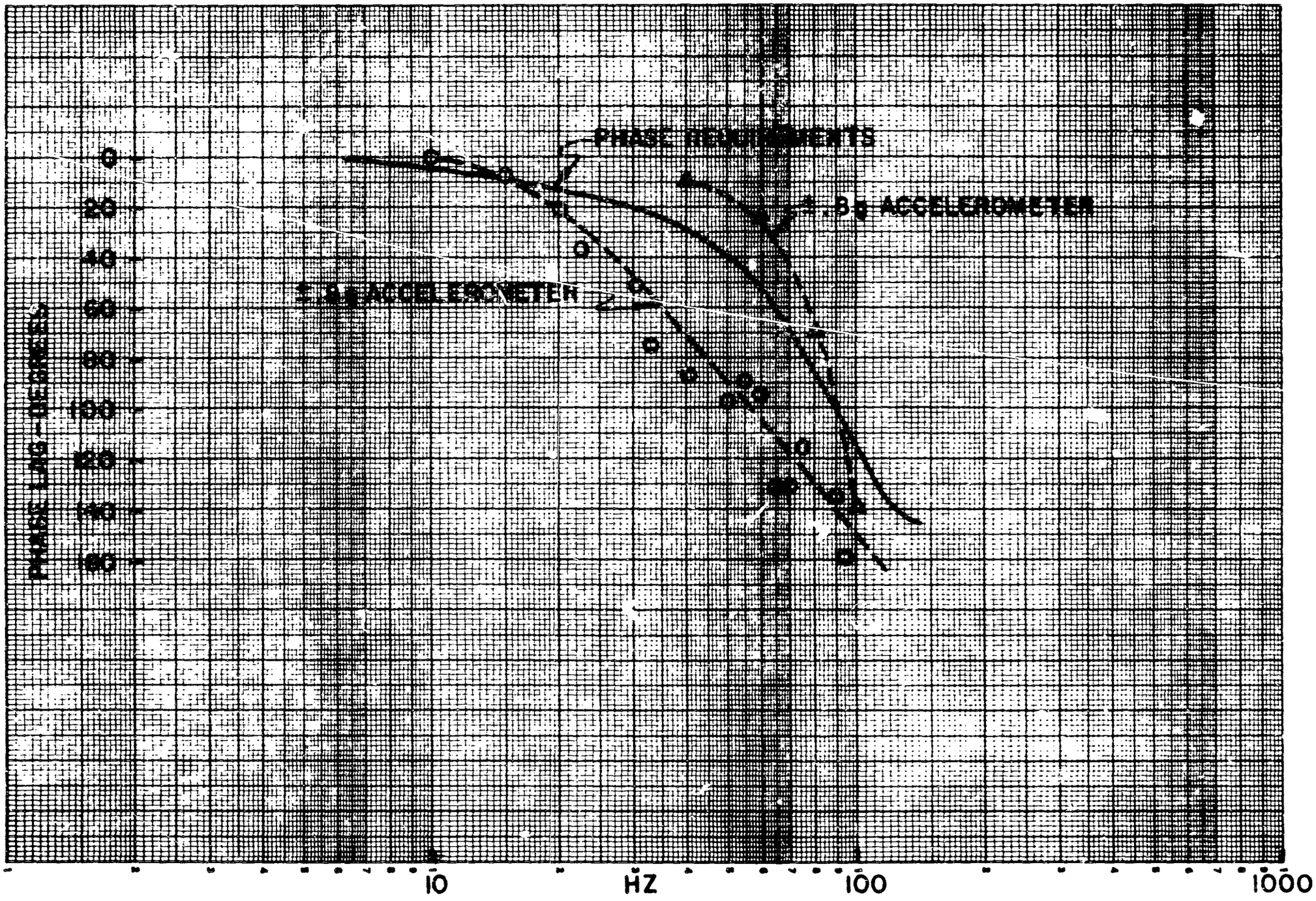


FIG. 2.7 CLOSED LOOP PHASE DATA

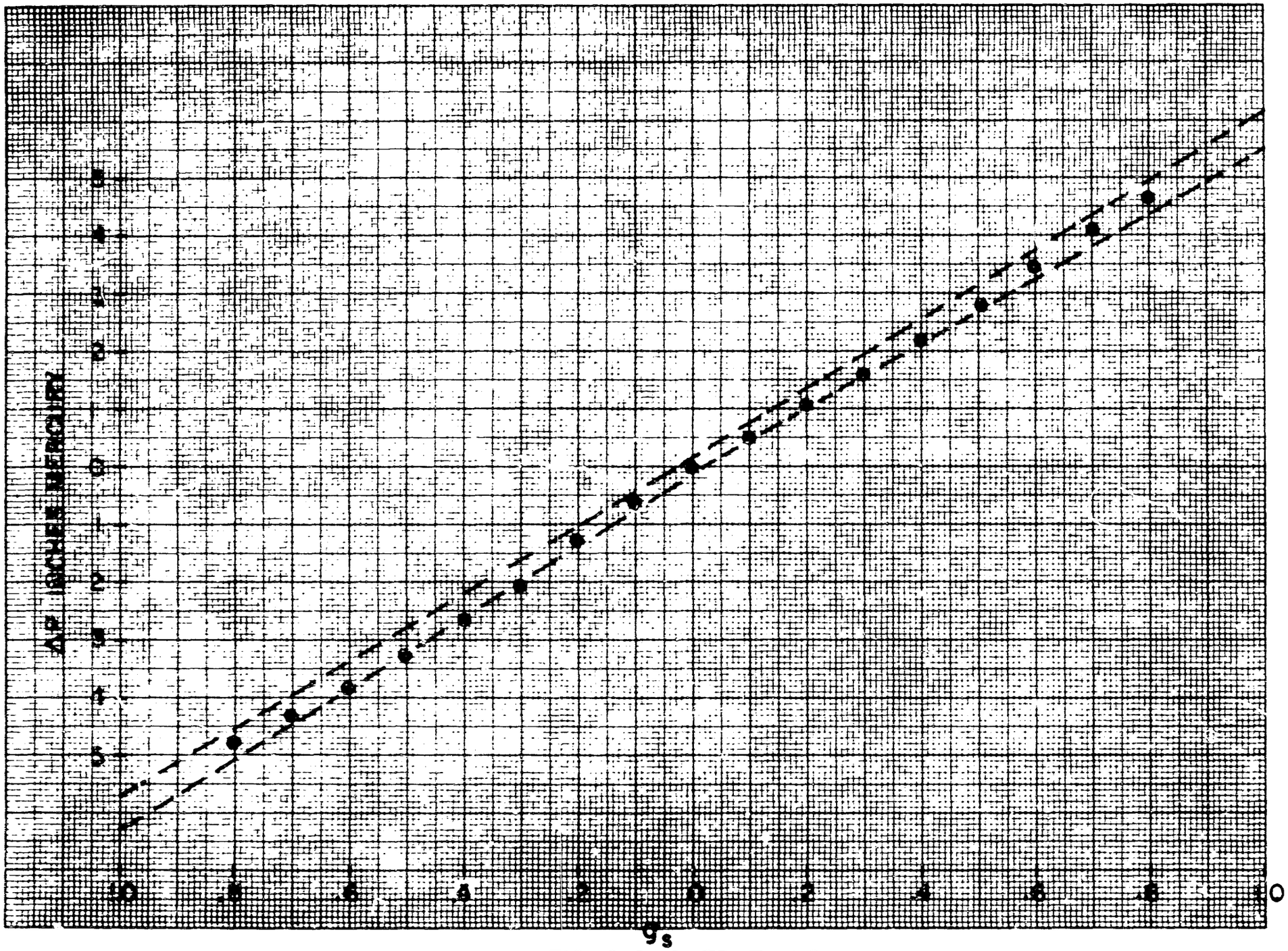


FIG. 2.8 OUTPUT VS g

## 3.0 SYSTEM ANALYSIS AND DESIGN

### 3.1 Transfer Function Derivation

A block diagram of the accelerometer is shown in Figure 3.1. The flexure and seismic mass is represented as a single spring-mass system. The resonant frequency of the flexure and mass ( $\omega_n$ ) is equal to $\left(\frac{K_f}{W/g}\right)^{\frac{1}{2}}$, the damping factor $\zeta$ is the inherent damping of the flexure, it will normally be less than .01 and for all practical purposes can be neglected. The system damping required is provided by the fluidic lead-lag circuit shown as a single lead followed by a lag break. The gain term G includes the total proportional gain of the fluidic circuit. The block labeled "circuit lag" represents transport lags due to path length and phase lag resulting from time constants in the power amplifier and pick-off amplifiers. The break frequencies resulting from these time constants will occur beyond system cross over and can be lumped into one equivalent time constant.

The open loop transfer function in terms of force acting on the mass is:

1. $$\frac{F_o}{F} = \frac{K_n A_n G \quad (1+TS) \quad \epsilon^{-j\omega T_T}}{K_f \quad (1+T_1 S) \quad (1+T_2 S) \quad \left(\frac{1+2\zeta S}{\omega_n} + \frac{S^2}{\omega_n^2}\right)}$$

$F_o$ is the output force and F is the applied force.

The closed loop transfer function in terms of output pressure ( $\Delta P_o$ ) and applied $g_a$-($^a i/g$ ) is:

2. $$\frac{\Delta P_o}{a_{i/g}} = \frac{\frac{WG\ (1+TS)}{K_f\ (1+T_1 S)\ (1+T_2 S)\ \left(\frac{1+2\zeta S}{\omega_n} + \frac{S^2}{\omega_n^2}\right)}}{1 + \frac{K_n A_n G\ \ (1+TS)}{K_f\ (1+T_1 S)\ (1+T_2 S)\ \left(\frac{1+2\zeta S}{\omega_n} + \frac{S^2}{\omega_n^2}\right)}}$$

If the open loop transfer function (equation 1) is much larger than unity equation 2 reduces to:

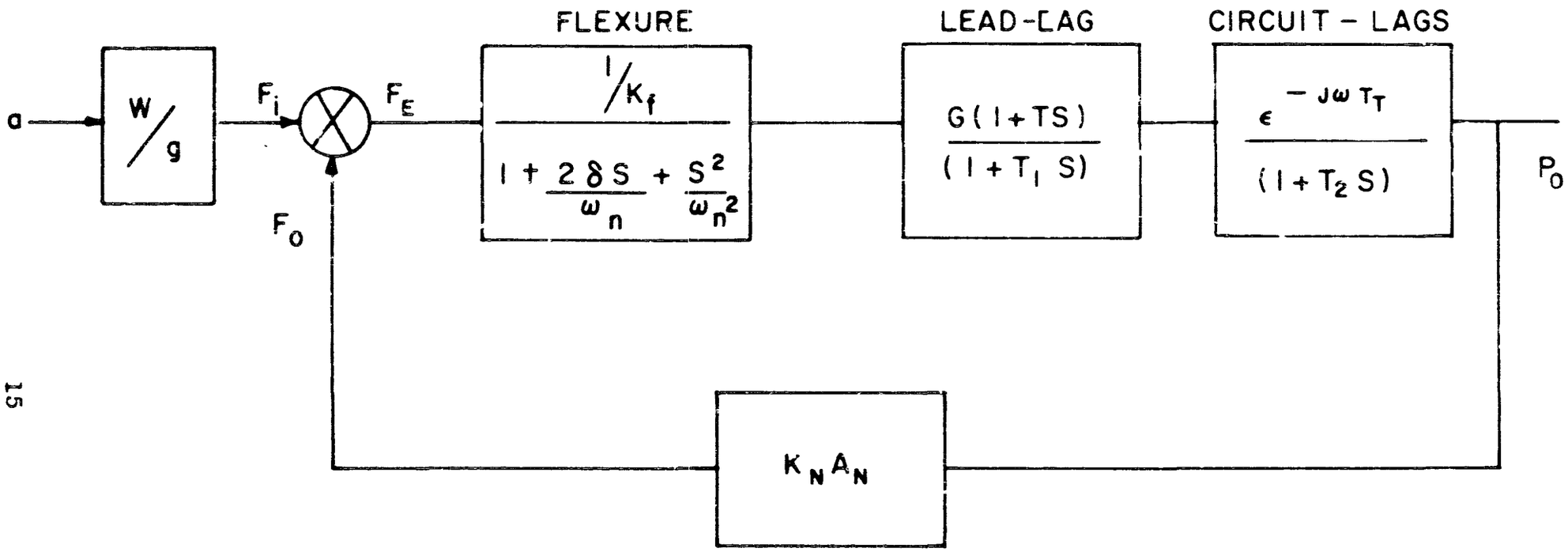


$K_f$ — FLEXURE GRADIENT
$\omega_n$ — RESONANT FREQ. OF FLEXURE
G — PROPORTIONAL GAIN
W — WEIGHT OF SEISMIC MASS
$K_N$ — NOZZLE FORCE COEFFIENT
$A_N$ — NOZZLE AREA
$T_T$ — TRANSPORT LAG

FIG. 3.1 PROPORTIONAL (PLUS LEAD-LAG)

3. $$\frac{\Delta P_o}{a_{i/g}} = \frac{W}{K_n A_n}$$

With sufficiently high loop gain the scale factor is a function of only the seismic mass and the nozzle area and its force coefficient.

A practical mechanization of an accelerometer as described by equation #1 will have to satisfy certain minimum band width criteria which are dependent on the range and maximum permissable flexure deflection. These criteria can be deduced by referring to the simplified diagram shown in Figure 3.2. The proportional loop gain $\frac{K_n A_n G}{K_f}$ should be as high as possible to make the accelerometer scale factor dependent on only the mass and nozzle characteristics. In a practical device the proportional loop gain should be greater than 10. The flexure has negligible damping, hence the mass displacement is acceleration limited in the frequency range where the system comprised only of the flexure and mass and proportional gain goes through unity gain. If it is assumed that this lead break in the damping loop occurs beyond crossover then $\omega_b$ becomes the minimum cross over frequency of the accelerometer. From the Bode diagram,

4. $$\omega_o = \left(\frac{K_n A_n G}{W/g}\right)^{\frac{1}{2}} = \left(\frac{K_f}{W/g}\right)^{\frac{1}{2}} \quad \text{(loop gain)}$$

Now considering the actual mechanization of the accelerometer there will be a maximum linear range or operating range of the fluidic circuits which can be related back to a maximum flexure displacement. ( $D_{max}$).

Now using equation 3 and noting that $\Delta P_o = DG$

5. $$\frac{D}{\left(a_{i/g}\right)} = \frac{W}{K_n A_n G}$$

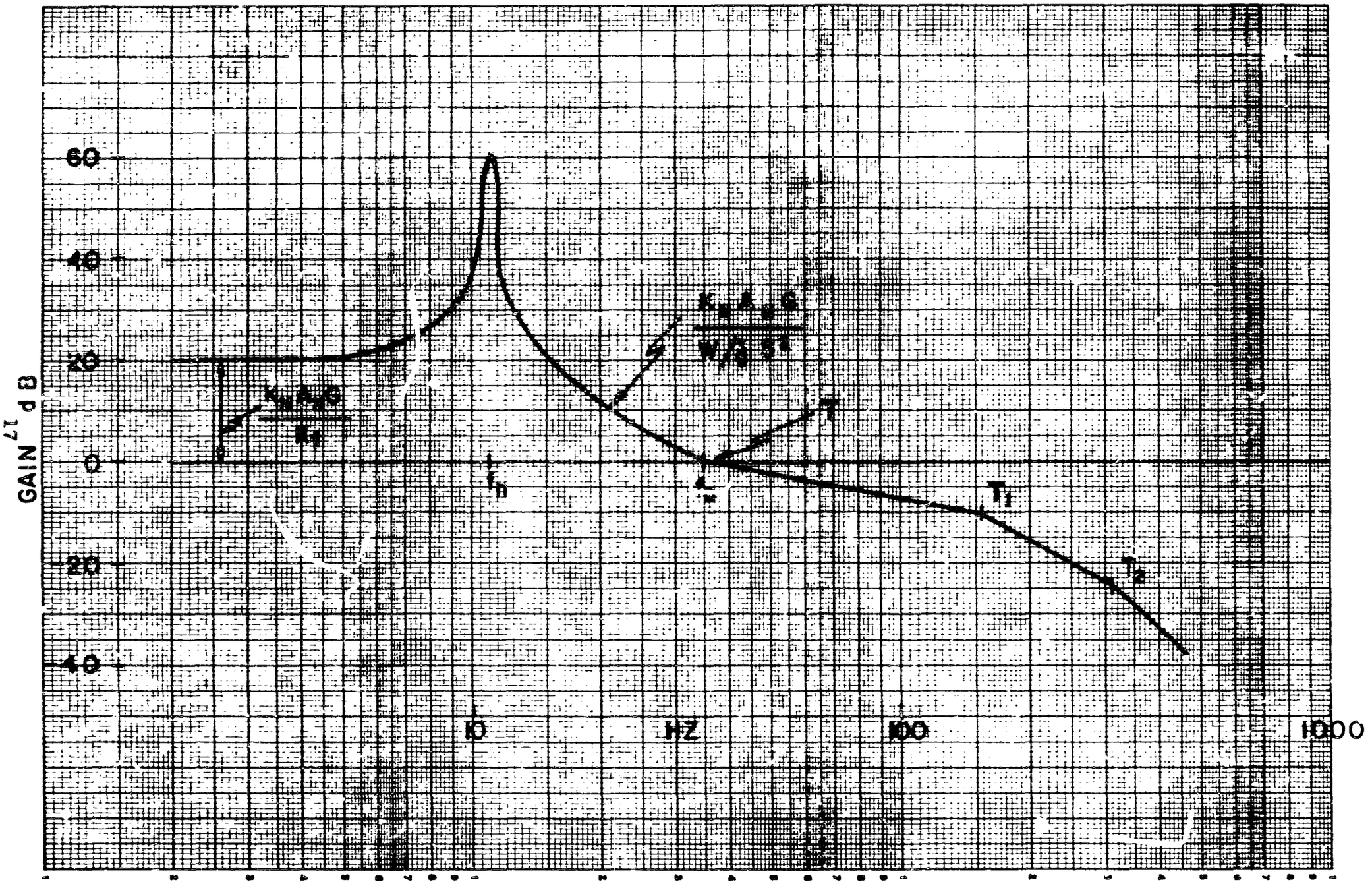


FIG. 3.2 PROPORTIONAL PLUS LEAD-LAG

To satisfy criteria that $D \lesssim D_{max}$ at the maximum applied g ($g_r$)

6. $$\frac{D_{(max)}}{g\ g_r} \lesssim \frac{W/g}{K_n A_n G}$$

Substituting into equation 4.

7. $$\omega_0 \gtrsim \left(\frac{g\ g_r}{D_{(max)}}\right)^{\frac{1}{2}}$$

Equation 7 states that the system bandwidth must be greater than $\omega_0$ and that $\omega_0$ is a function of only the g range the accelerometer is designed for and the permissable flexure deflection when maximum g s are applied. In an actual mechanization $D_{(max)}$ will normally be set by the physical size of the jet nozzles and pick-off amplifier, hence once the pick-off amplifier configuration is selected the minimum system bandwidth is directly proportional to the square root of the g range.

By manipulating equation 4 and 6 it can be shown that to satisfy the minimum bandwidth

8.
$$\text{loop gain} = \left(\frac{g_r}{D_{(max)}}\right)\frac{W}{K_f} = \left(\frac{g_r}{D_{(max)}}\right)\frac{g}{\omega_\eta^2}$$

where $\omega_\eta$ is the resonant frequency of the flexure.

The primary parameters of the accelerometer can now be determined in terms of the design goals and geometry of the pick-off amplifiers. The particular pick-off amplifier used permits a $D_{(max)}$ of .008 inches. A loop gain of 10 was selected to satisfy linearity requirements.

9. $$\omega_\eta = \left(\frac{g_r g}{D_{max}}\right)^{\frac{1}{2}} = \left[\frac{386}{(.008)10}\right]^{\frac{1}{2}} = 69 \text{ rad/sec}$$

and

10. $$\omega_o \geq \left(\frac{gg_r}{D_{max}}\right)^{\frac{1}{2}} = \left(\frac{386}{.008}\right)^{\frac{1}{2}} = 220 \text{ rad/sec}$$

The minimum crossover of $\omega_o$ is a limit which is approached as system damping approaches zero. A practical minimum crossover will be approximately 50% higher or 330 rad/sec. The design goal bandwidth based on intended application of the accelerometer is 500 rad/sec. The minimum system band width is then dictated by the design goal bandwidth rather than the design goal of ± 1g on range.

The particular mechanization shown in Figure 3.1 does not lend itself to a high g range -- i.e. a high range will demand excessive system bandwidths. It is estimated that current "state-of-the-art" amplifiers will limit $\omega_o$ to a maximum of 250 rad/sec. The maximum range can then be deduced from equation 7.

11. $$g_r = \frac{\omega_o^2 D_{(max)}}{g} = \frac{(250)^2 (.008)}{386} = \pm 1.3g$$

An accelerometer with only proportional gain and lead-lag for damping will then be limited to relatively low g applications.

A method of extending the range independently of bandwidth is illustrated by the block diagram of Figure 3.3. Mechanization of this system requires the addition of an integrator or lag-lead circuit as shown by the simplified Bode plot of Figure 3.4. The minimum system bandwidth is now:

12. $$\omega_o \geq \left[\left(\frac{T_1}{T_o}\right) \frac{gg_r}{D_{max}}\right]^{\frac{1}{2}}$$

and

13. $$g_r = \frac{\omega_o^2 D_{max}}{g} \left(\frac{T_o}{T_1}\right)$$

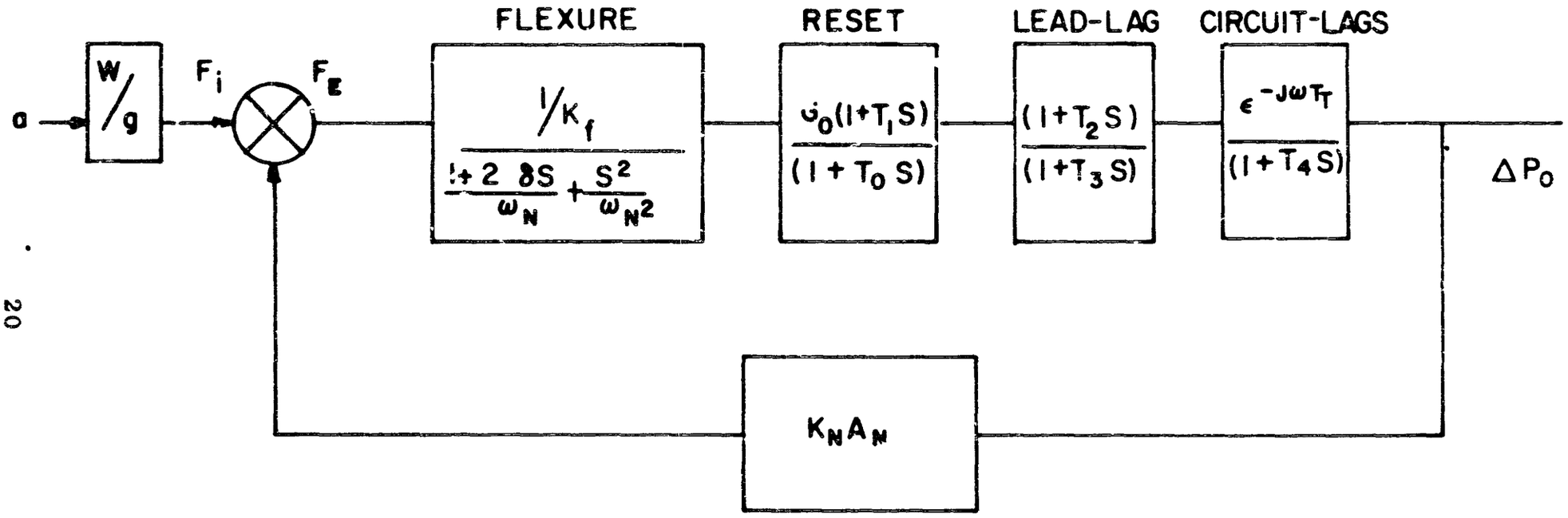


$G_c$ – STEADY STATE GAIN

$T_0$ – RESET TIME CONSTANT

FIG. 3.3 PROPORTIONAL PLUS LEAD-LAG PLUS RESET

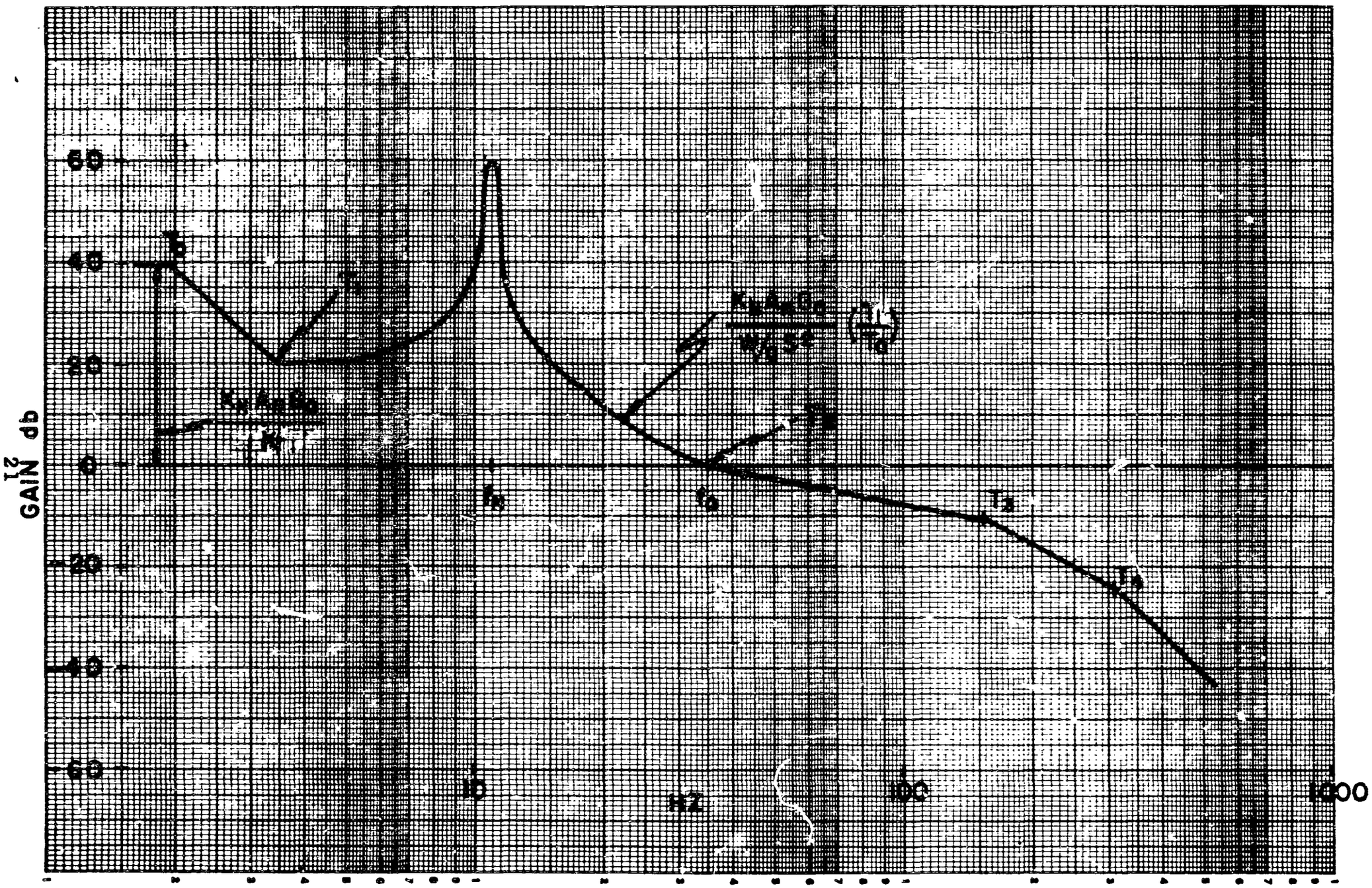


FIG. 3.4 PROPORTIONAL PLUS LEAD-LAG, PLUS RESET

Comparing equations 13 and 11, it is apparent that the range is extended by the ratio of $\left(\frac{T_o}{T_1}\right)$. A range of 20:1 in time constants can be quite readily achieved. This will extend the g capability of the accelerometer to the ± 20g range. Another advantage of the integrator is that the maximum steady state loop gain is also increased by the ratio of $\left(\frac{T_o}{T_1}\right)$. This results in improved stability and linearity of scale factor.

Mechanization of the second system is considerably more complex than the single proportional system and it should be selected only if required to meet the system design goals.

## 3.2 Linearity and Scale Factor Stability

The steady state scale factor from equation #2 is:

$$14. \quad \frac{\Delta P_o}{\left(a_{i/g}\right)} = \frac{WG/K_f}{1 + \frac{K_n A_n G}{K_f}}$$

The variation of scale factor with a change in $K_f$ is given by:

$$15. \quad d\left(\frac{\Delta P_o}{a_{i/g}}\right) = \frac{WG \; d(K_f)}{K_f^2\left(1 + \frac{K_n A_n G}{K_f}\right)^2}$$

Expressing equation 15 in terms of percent change:

$$16. \quad d\left(\frac{\Delta P_o}{a_{i/g}}\right)\% = \frac{d(K_f)\%}{1 + \frac{K_n A_n G}{K_f}}$$

$\frac{K_n A_n G}{K_f}$ is the steady state loop gain. When the loop gain is much greater than unity it is apparent that the influence of flexure gradient on scale factor or linearity is reduced by a factor equal to the loop gain. For example, the spring constant of a stainless steel flexure will change approximately 2% per 100°F, if a loop gain of 10 is used this will reflect only a .2%/100°F change into the scale factor.

The fluidic amplifier gain G is also subject to unpredictable change-- it will change almost directly with supply pressure.

The relationship between scale factor and gain is given by:

$$17.\quad d\left(\frac{\Delta P_o}{a_{i/g}}\right) = -\frac{W\ d(G)}{K_f\left(1+\frac{K_n A_n G}{K_f}\right)^2}$$

expressed in percent change:

$$18.\quad d\left(\frac{\Delta P_o}{a_{i/g}}\right)_{\%} = -\frac{d(G)_{\%}}{\left(1+\frac{K_n A_n G}{K_f}\right)}$$

The effect of amplifier gain on scale factor has again been reduced by a factor equal to the loop gain. With a loop gain of 10 supply pressure changes of 10% will give changes in scale factor on the order of 1%.

If the loop gain is sufficiently high the scale factor is given by:

$$\therefore \left(\frac{\Delta P_o}{a_{i/g}}\right) = \frac{W}{K_n A_n}$$

On a percentage basis there will be a one to one relationship between scale factor change and change in the nozzle coefficients $K_n$ and $A_n$.

The effect of misalignment and other sources of bias are also reduced by loop gain.

The relationship between the pressure required to satisfy a force balance and an initial misalignment $D_o$ between jet pipe and pick-off amplifier is given by:

$$20.\quad \Delta P_o = \frac{G\ D_o}{\left(1+\frac{G\ K_n A_n}{K_f}\right)}$$

expressed as a ratio of the range.

21. $$g_B = g_r \frac{(D_o/D_{max})}{\left(1+ \frac{G K_n A_n}{K_f}\right)}$$

Using typical values of $D_{max}$ = .008" and $g_r = \pm$ 1g and a loop gain of 10, the bias $g_B$ resulting from a .001" misalignment is .0125g.

Another common source of bias is dissymmetry in the fluid amplifier. A differential pressure will be present on the output when the input signal is zero. The resulting closed loop bias is given by:

22. $$\Delta P_f = \frac{\Delta P_B}{\frac{(1+K_n A_n G)}{K_f}}$$

$\Delta P_B$ is the open loop bias pressure appearing on the output of the amplifier and $\Delta P_f$ is the closed loop bias pressure. For example, if $\Delta P_B$ is 10% of the output pressure required for maximum g range and the loop gain is 10, then the bias g will be 1% of the full range.

## 4.0 HARDWARE DESIGN

### 4.1 General Design Parameters

The major design parameters of the accelerometer are fairly well established once the steady state loop gain requirements and pick-off amplifier geometry have been determined.

The approximate size of the pick-off amplifier can be established by consideration of equation 7 in section 3.1. The amplifier should not be so small that the minimum bandwidth to satisfy range exceeds the design goal bandwidth. The numerical example given in section 3.1 indicates that the pick-off amplifier nozzle or the inner diameter of the jet pipe should not be less than .008 inches. The design equations show loop gain to be inversely proportional to flexure gradient. Flexure gradient should then be as low as possible, the jet pipe and hence the pick-off amplifier should be as small as possible. The logical choice of amplifier and jet pipe are then the smallest which are consistent with bandwidth consideration. A standard General Electric proportional amplifier very closely matches the minimum size and was chosen as the pick-off amplifier. An .01" inside diameter jet pipe is optimum for use with this amplifier.

From equation 9, section 3.1, the natural frequency of the flexure is established at approximately 11 HZ.

A loop gain of at least 10 was chosen to minimize the effects of temperature, mechanical and fluidic bias's and supply pressure changes. The open loop gain and phase margin required to meet the design goals on response and phase lag are shown in Figure 4.1. Phase leads of 50 to 60 degrees are required in the frequency band around cross over. This phase lead must be supplied by the fluidic circuits in that flexure damping is negligible.

### 4.2 Flexure Design

A sketch of the seismic mass flexure is shown in Figure 4.2. The primary flexure consists of a stainless steel tube with an ID of .01" and a wall thickness of .004". The flexure is stiffened along the insensitive axis by two unstressed stainless guy wires. The

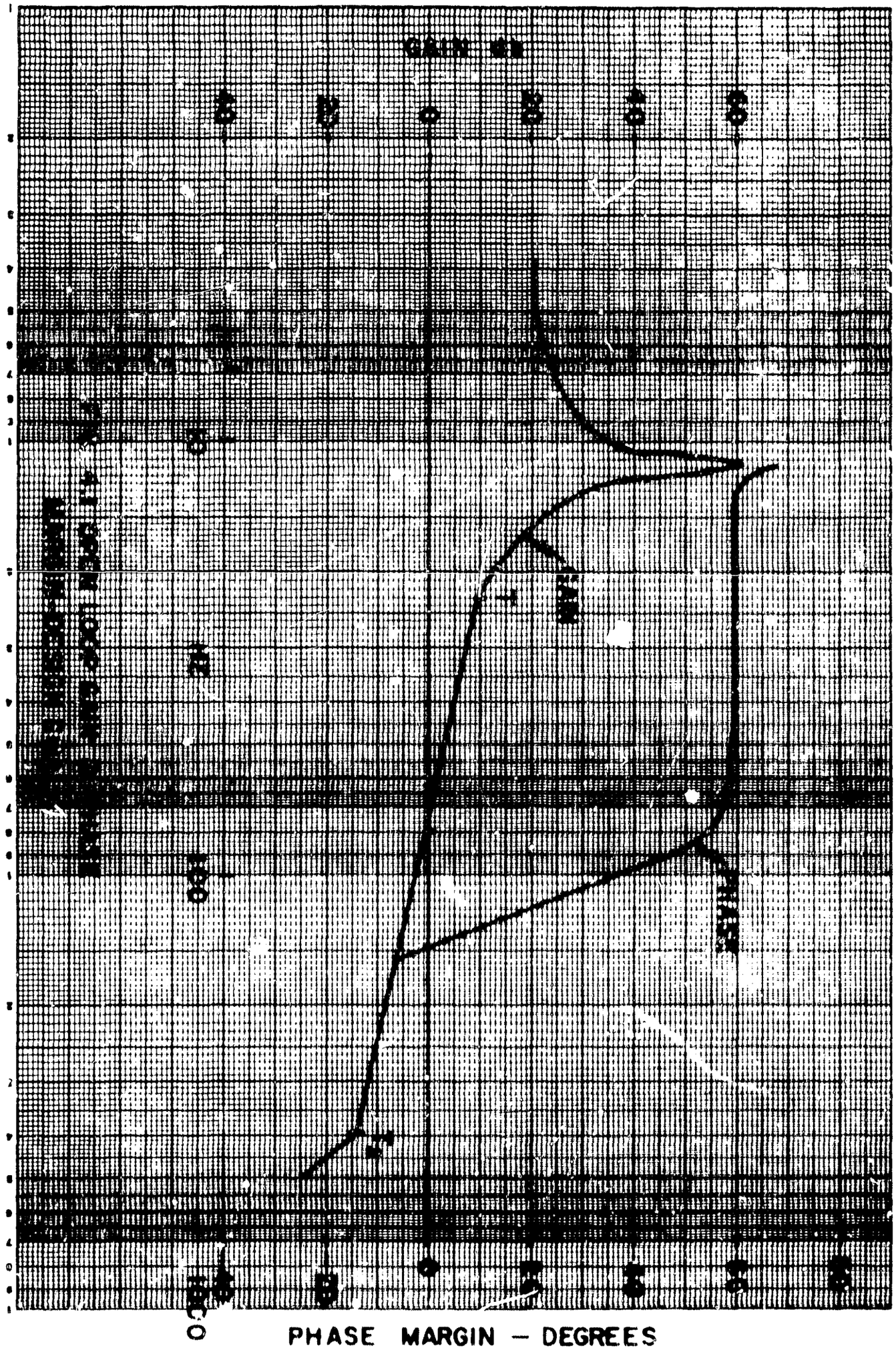
GAIN dB
PHASE MARGIN – DEGREES

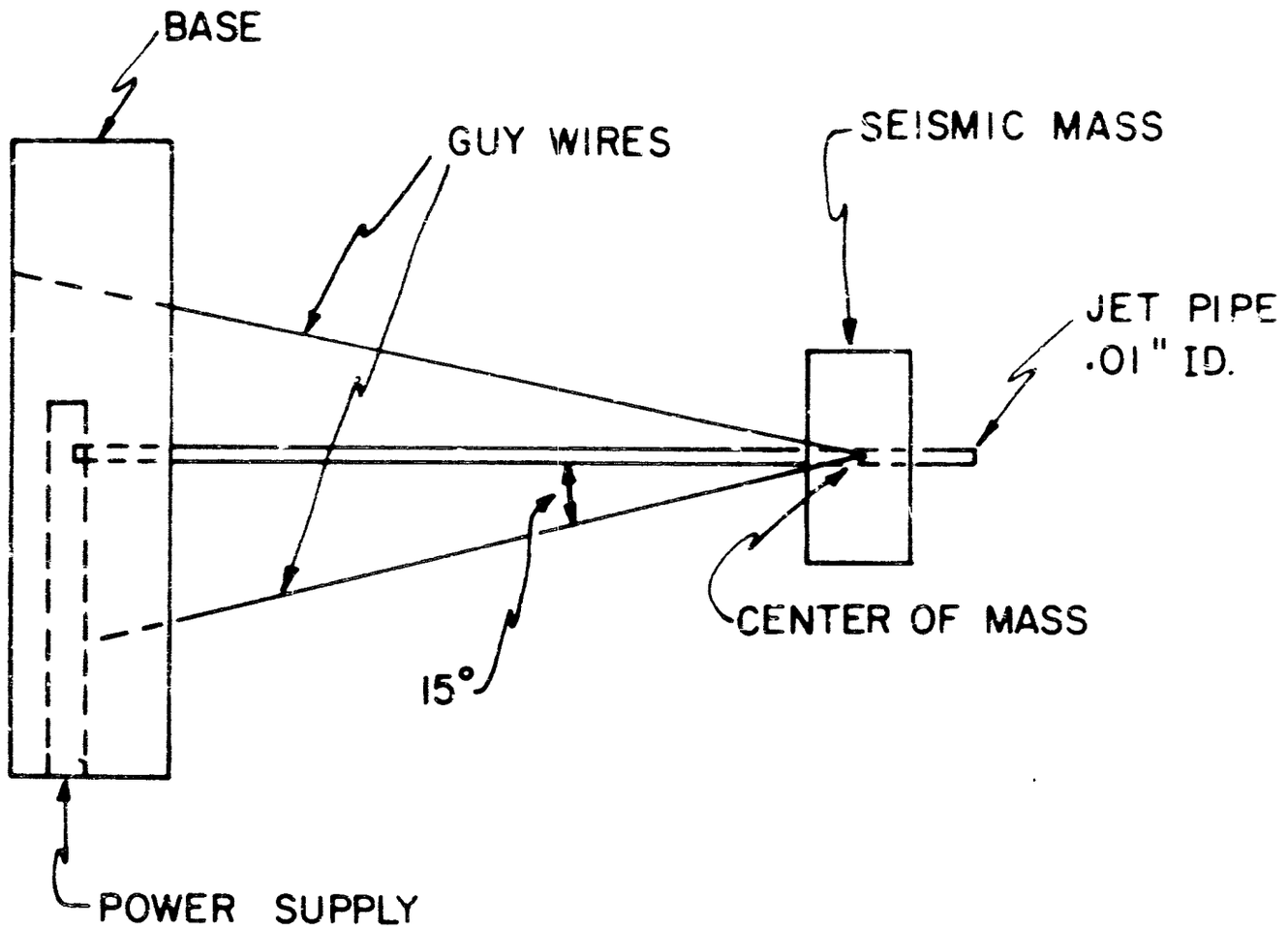


FIG. 4.2 SEISMIC MASS

resultant forces from the guy wires and flexure are applied through the center of mass to minimize coupling of forces acting along the insensitive axis. This particular design has a high ratio of stiffness along the insensitive axis to stiffness along the sensitive axis.

The spring gradient of a hollow tube flexure is given by:

$$23. \quad K_f = \frac{3EI}{l^3} = \frac{3E\pi D_i^4}{8l^3k}\left(1 + {}^3/_k + {}^4/_{k^2} + {}^2/_{k^3}\right)$$

I = cross sectional moment of inertia
E = modules of elasticity
l = length
$D_i$ = inside diameter of tube
k = ratio of ID to wall thickness

Using a stainless tube with an ID of .01 inches and a wall thickness of .004" the gradient is .38 lbs/in for a one inch length. This gradient is increased to .41 lbs/in for a one inch flexure length when factoring in the cross sectional moment of the guy wires.

The weight of the seismic mass was established at .007 lbs from the output amplifier considerations. The gradient required to get a 11 HZ resonance is then:

$$24. \quad K_f = \frac{4f_o^2 \pi^{-2} W}{g} = .086 \ \#/in$$

And the required length is:
$l = (.41/.086)^{1/3} = 1.67$ inches

The gradient along the insensitive axis is given by:

25.

$$K_{\perp} = K \sin^2\theta$$

K-gradient of one guy wire in tension
$\theta$-angle between the guy wire and primary flexure.

For the specific design K is equal to 510 lbs/in and an angle of $15^{o}$ was selected for $\theta$.
then:

$$K_f = 510\ (.258)^2 = 34\ \#/in$$

The ratio of gradient along the two axis is then 34/.086= 400:1. Drawing #542C601 in the appendix shows the farbication details for the flexure assembly. The flexure on the delivered hardware deviates from the drawing in that the parts were joined by soft solder rather than copper braze. Attempts at joining the parts by copper brazing were unsatisfactory in that the resulting flexure had either very little initial restraint along the insensitive axis or exhibited a snap action along the sensitive axis. The probable cause is uneven stressing of the wires during brazing and subsequent cooling.

The soft solder presented no fabrication problem and does give a satisfactory assembly for temperatures up to $300^{o}$F. Extension of the temperature range will require perfecting of the high temperature braze technique.

### 4.3 Nulling Nozzle and Output Amplifier Design

The overall design philosophy on the accelerometer is to provide sufficient loop gain so that the accelerometer characteristics are determined entirely by the feedback gain and seismic mass. The feedback is through the nulling nozzle, hence the accelerometer linearity and scale factor are set almost entirely by the effective area and force coefficient of the nozzles.

The force developed by a nozzle on a flat surface varies from the static pressure force (product of area and supply pressure) at very small nozzle to surface gaps to a value twice the static pressure force at large gaps. For this application it is necessary that the nozzle force be independent of gap and that the force be as high as possible for a given supply pressure. Both these considerations dictate operating with a large gap. When the gap is greater than several nozzle diameters the force is essentially independent of gap and has reached its maximum value. This is illustrated by Figure 4.3 which is a plot of measured force on a flat surface vs. gap. A nominal gap of 2.5 times the nozzle diameter was established as the operating gap.

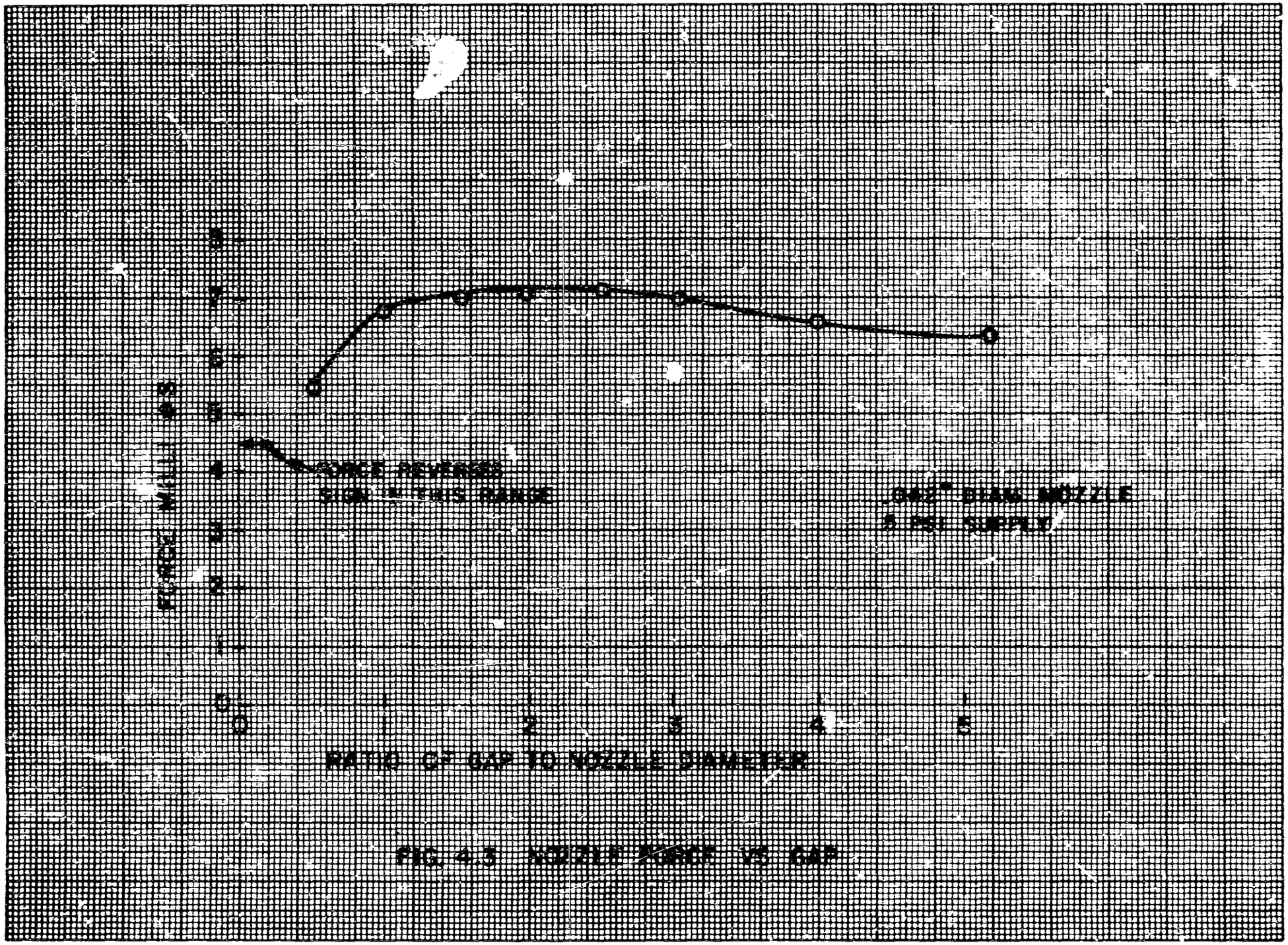


FIG. 4.3 NOZZLE FORCE VS GAP

The linearity of the force vs. pressure relationship was determined by tests on various nozzle configurations. The tests consisted of measuring pressure recovery at the jet center line as well as force measurements.

Pressure measurements were made with a small pitot tube located 2.5 nozzle diameters from the nozzle exit. The results from two configurations are plotted in Figure 4.4. The recovery pressure is lower with the orifice -- however the pressure recovery in both instances is directly proportional to supply pressure which indicates that there are no non-linear losses occurring in the nozzles.

Figure 4.5 shows the relationship between the force produced on a flat plate and supply pressure. The relationship is linear even though there is a considerable discrepancy between the measured force and the theoretical value of twice the static force. The force coefficient can be increased significantly by directing the jet at a hemispherical cup as shown in Figure 4.5. However, the linearity and stability are definitely worse than for a flat surface.

The matching of the power amplifier to the nulling nozzle is based on maximizing the force for a given supply pressure and nozzle flow in the output amplifier. This will give the accelerometer the greatest g range for a given supply power. The optimum match can be established by determining force vs. nozzle area for a given output amplifier. Figures 4.6 and 4.7 show both the pressure drop across the nulling nozzle vs. nozzle area and the force vs. nozzle area. There is a fairly well defined optimum operating point which is independent of supply pressure over the range tested. This point is where the area of the nulling nozzle is approximately equal to the nozzle area of the output amplifier. Referring to Figure 4.6 it is evident that the pressure drop across the nozzle is relatively low at the optimum operating point as compared to blocked load pressure recovery. It is then apparent that the output stage should not be operated with a nozzle which gives very high scale factors. It should be operated at about 50% of the maximum scale factor obtainable with very small nulling nozzles.

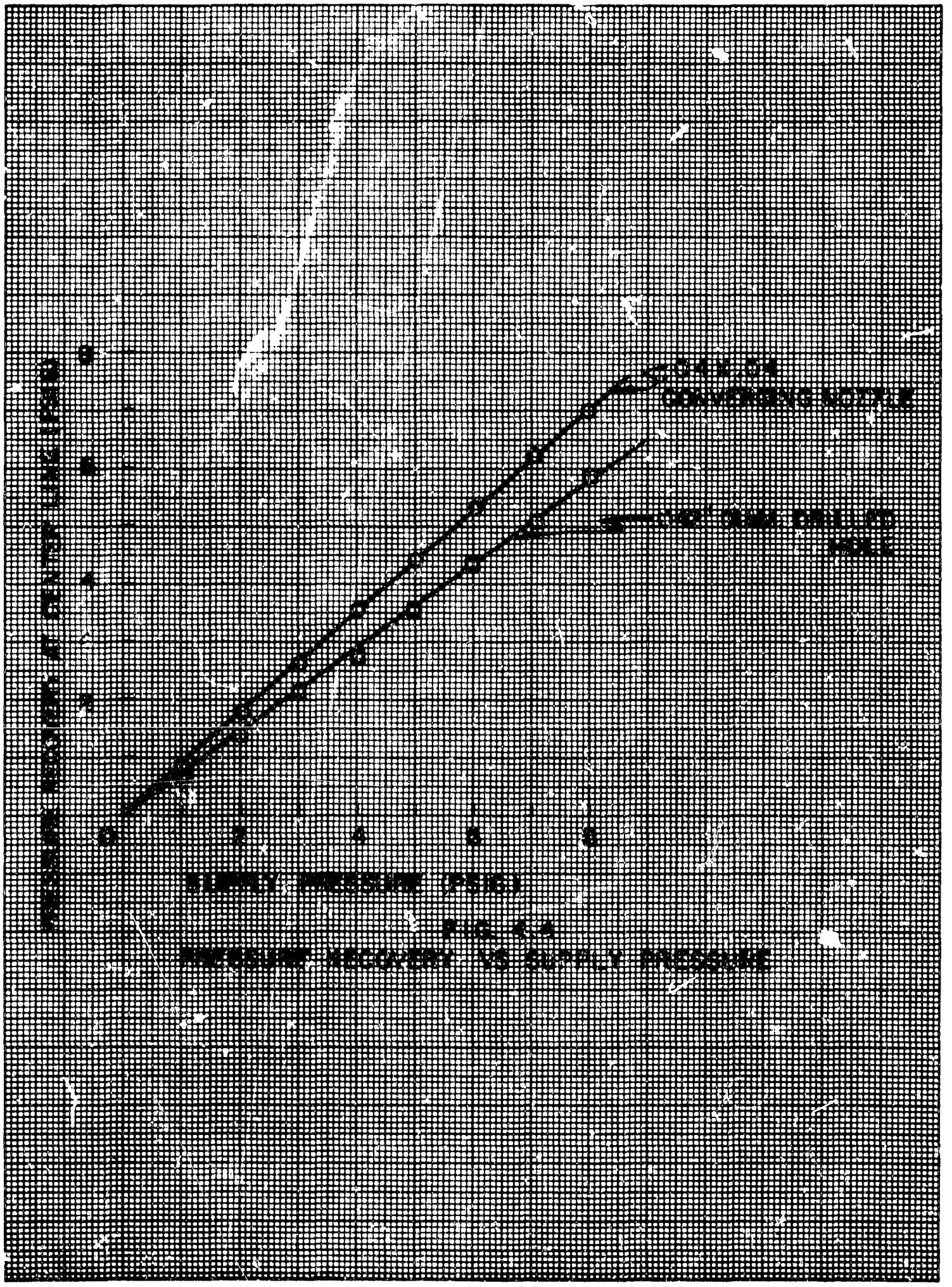


FIG. 4.4
PRESSURE RECOVERY VS SUPPLY PRESSURE

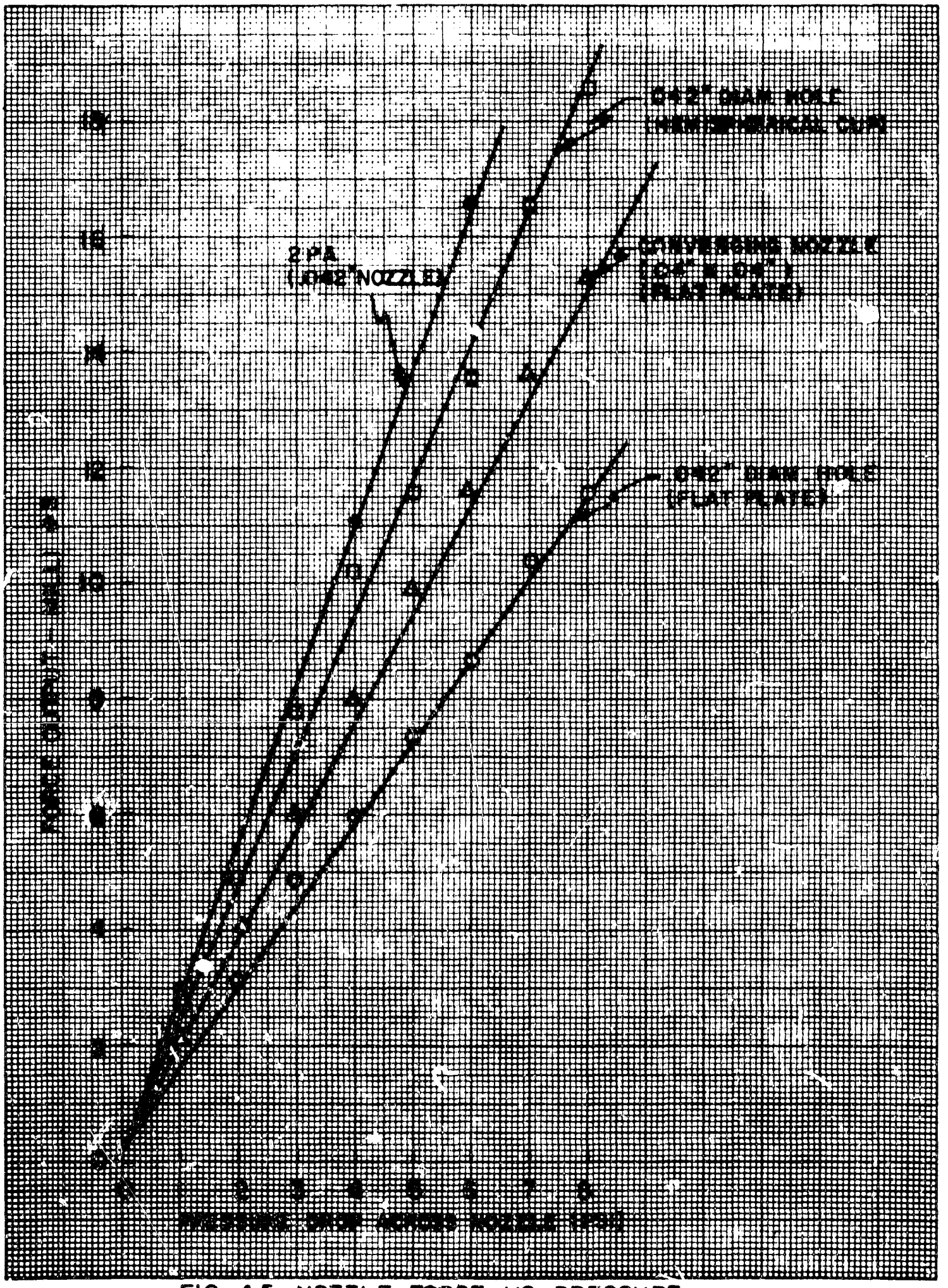


FIG. 4.5 NOZZLE FORCE VS PRESSURE

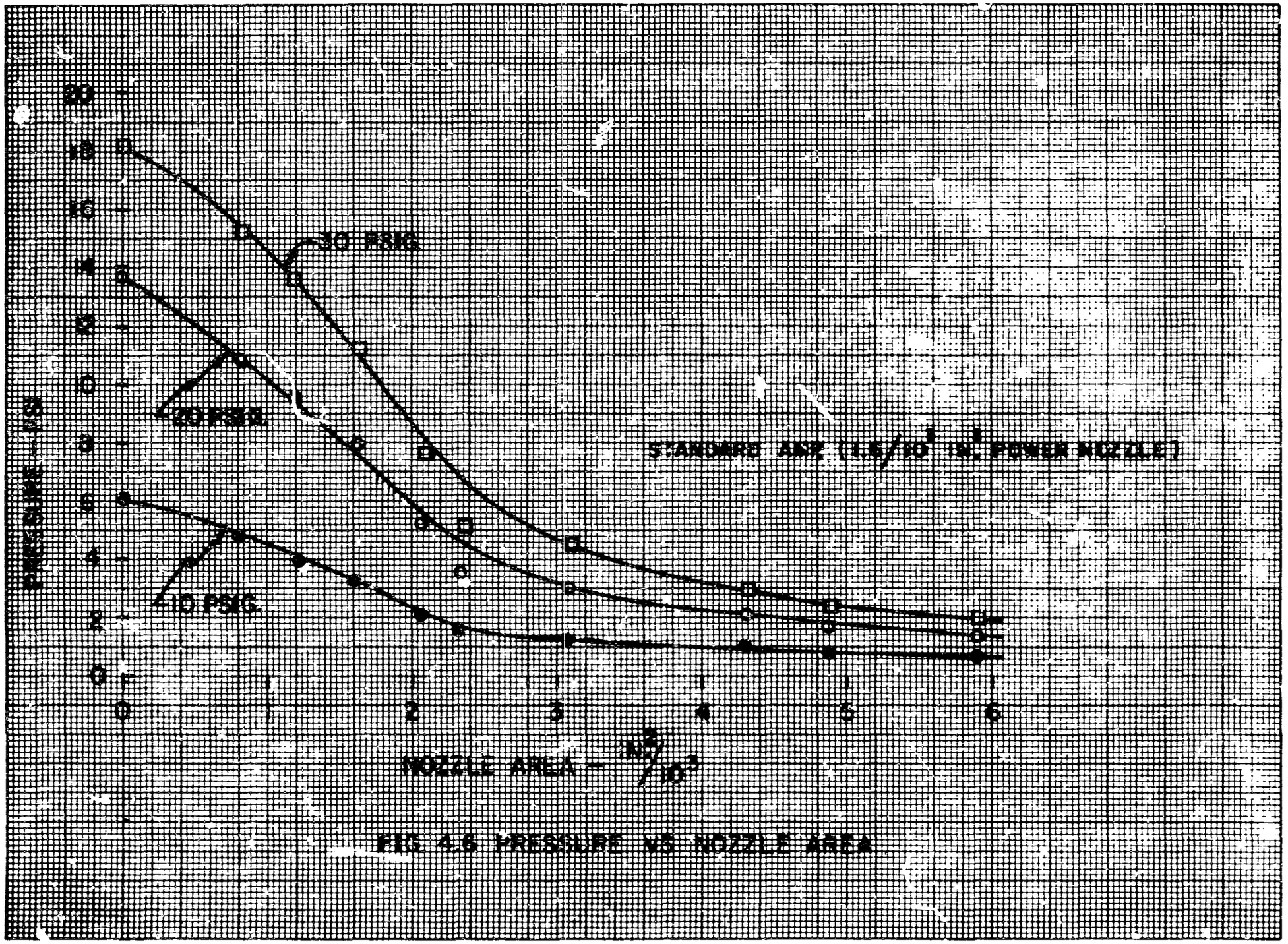


FIG 4.6 PRESSURE VS NOZZLE AREA

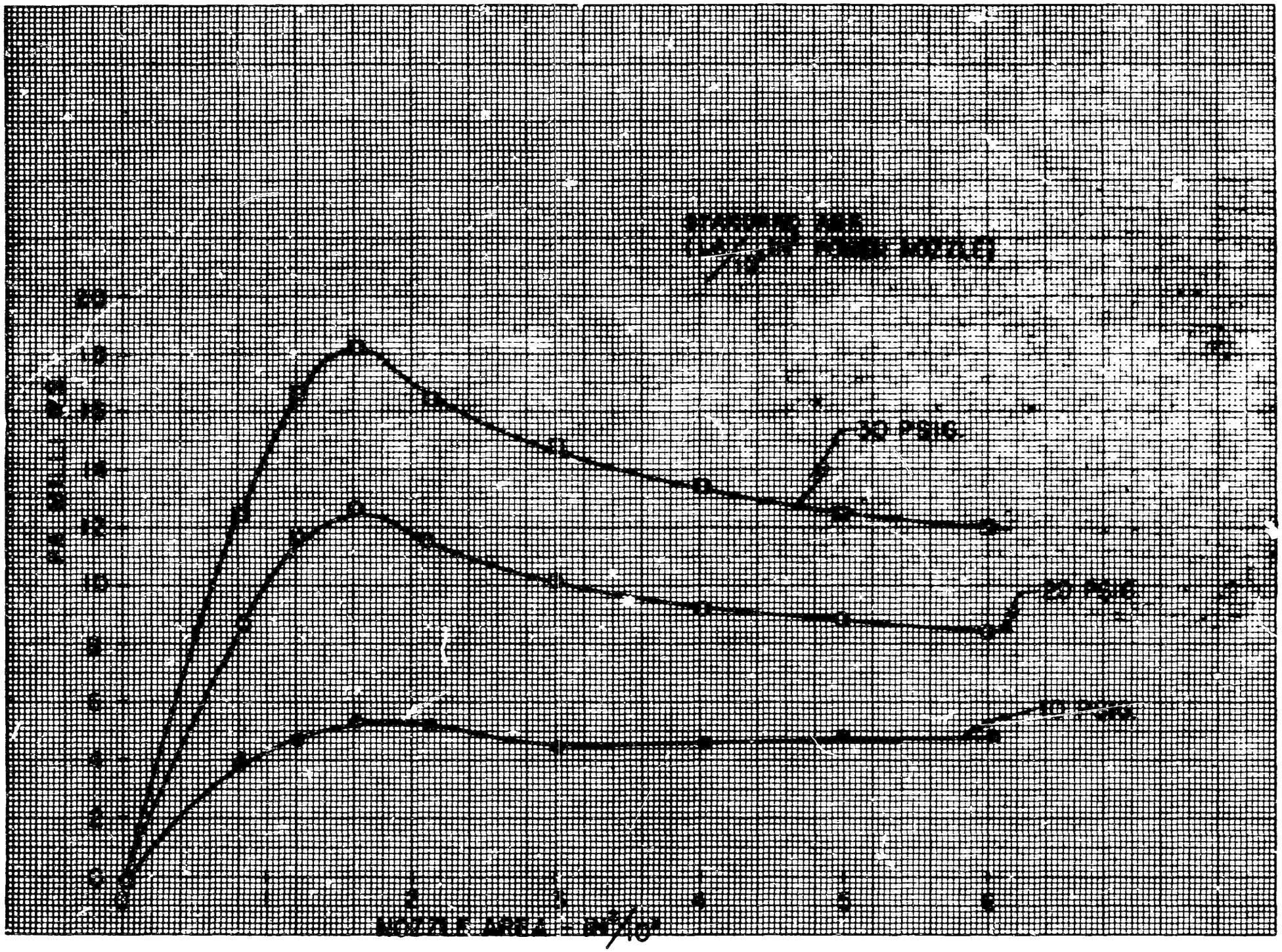


FIG. 4.7 FORCE VS NOZZLE AREA

The absolute size of the nulling nozzles is somewhat arbitrary. It is based on practical trade-offs between the flexure design and output amplifier. From the standpoint of the flexure the seismic mass wants to be large so that the relatively low resonant frequency can be obtained with a short, compact flexure. However, a large mass requires large nozzles to meet the specified g range, and from the standpoint of minimizing power in the output amplifier the mass and consequently nozzles should be as small as possible. A seismic mass of .007 lbs was selected as a reasonable compromise.

An output amplifier with a .0016 $in^2$ power nozzle driving a .0016 to .002 $in^2$ nulling nozzle gives a good operating force margin with this mass (see Figure 4.7) and the flexure design is reasonably compact.

The output amplifier is made up of standard amplifier laminations stacked to give a nozzle area of .0016 $in^2$ (.02" x .08'). The output amplifier is combined with a standard proportional pre-amplifier in one common module.

## 4.4 Lead-lag Circuit Design

Two approaches to the lead-lag circuit are shown in Figure 4.8. The circuit of Figure 4.8a is based on a standard proportional element with inductive shunts on the output. With this configuration the lead break is determined primarily by the ID of the tube used as the inductance, the lag break is determined by the total inductance or both the ID and length of the tube. The transfer function for this configuration is given by;

$$26. \qquad \frac{P_o}{P_i} = \frac{G_B R_S}{R_o} \; \frac{\left(1 + S\,\frac{L}{R_s}\right)}{\left(+ S\,\frac{L(R_o+R_i)}{R_o R_i}\right)}$$

$G_B$ - blocked load gain of amplifier

$R_S$ - resistance of tube used as inductance

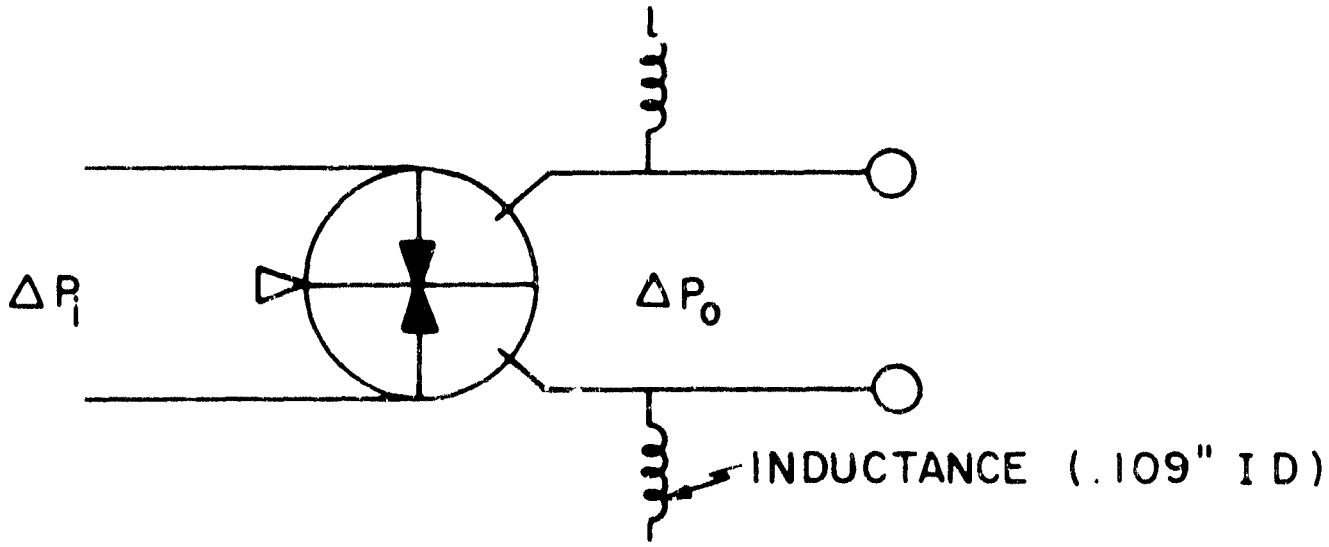


a. INDUCTIVE LEAD-LAG

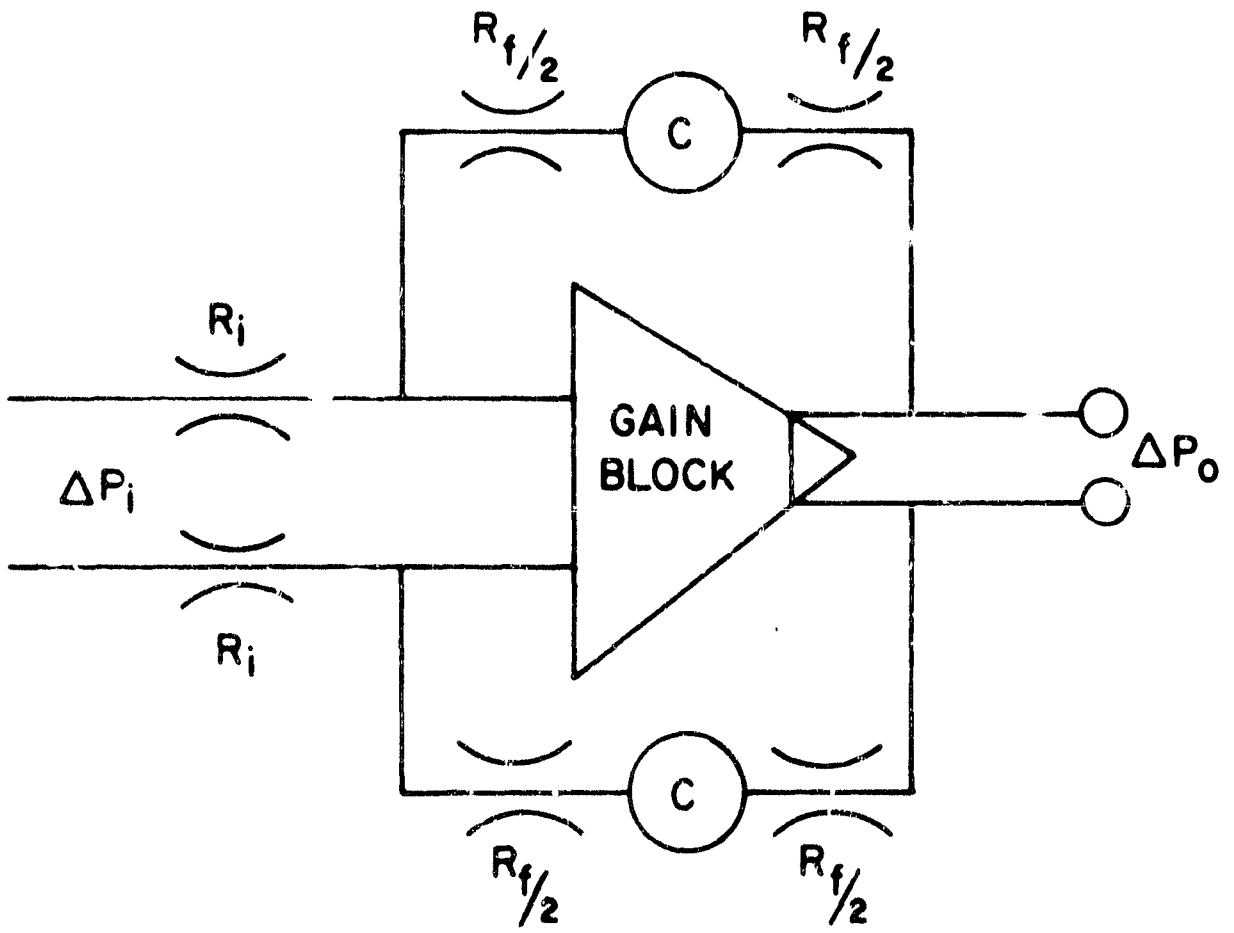


b. OPERATIONAL AMPLIFIER LEAD-LAG

FIG. 4.8 LEAD-LAG SCHEMATICS

$R_o$ - output impedance of amplifier

$R_i$ - input impedance of driver stage

L - inductance of tube.

Gain and phase data for this circuit are plotted in Figures 4.9 and 4.10. The top frequency limit is determined by the quarter wave length resonance of the tube used as the inductance. This approach is particularly attractive where very high bandwidths are needed. For example, with a 6 inch length of tube, phase leads of $52^{o}$ @ 200 HZ and $20^{o}$ @ 400 HZ were obtained. A 12" tube length is optimum for a system crossover in the vicinity of 100 HZ yielding a phase lead of $55^{o}$ at that frequency. Care must be exercised in applying this approach in that the circuit exhibits a damped resonance in the vicinity of the lag break.

The second approach consists of a standard operational amplifier with a lag circuit in the feedback. The lead time constant is determined by the resistance-capacity time constant in the feedback network. The lag break is determined by the amplifier loop gain -- the maximum upper limit is set by the maximum cross-over frequency of the amplifier. The transfer function is given by

27. $$\frac{P_o}{P_i} \quad \frac{R_f}{R_i} \quad \frac{\left(1+\frac{R_f c\ S}{4}\right)}{\left(1+\frac{R_f c\ S}{4(GH)}\right)}$$

$R_f$ - Total resistance in feedback path

$R_i$ - input resistance

C - capacitance

GH - loop gain

A plot of gain and phase shift are shown in 4.11. This circuit yields a phase lead of $60^{o}$ @ 100 HZ.

The operational amplifier approach was selected for this application primarily because its steady state characteristics are fixed and well known.

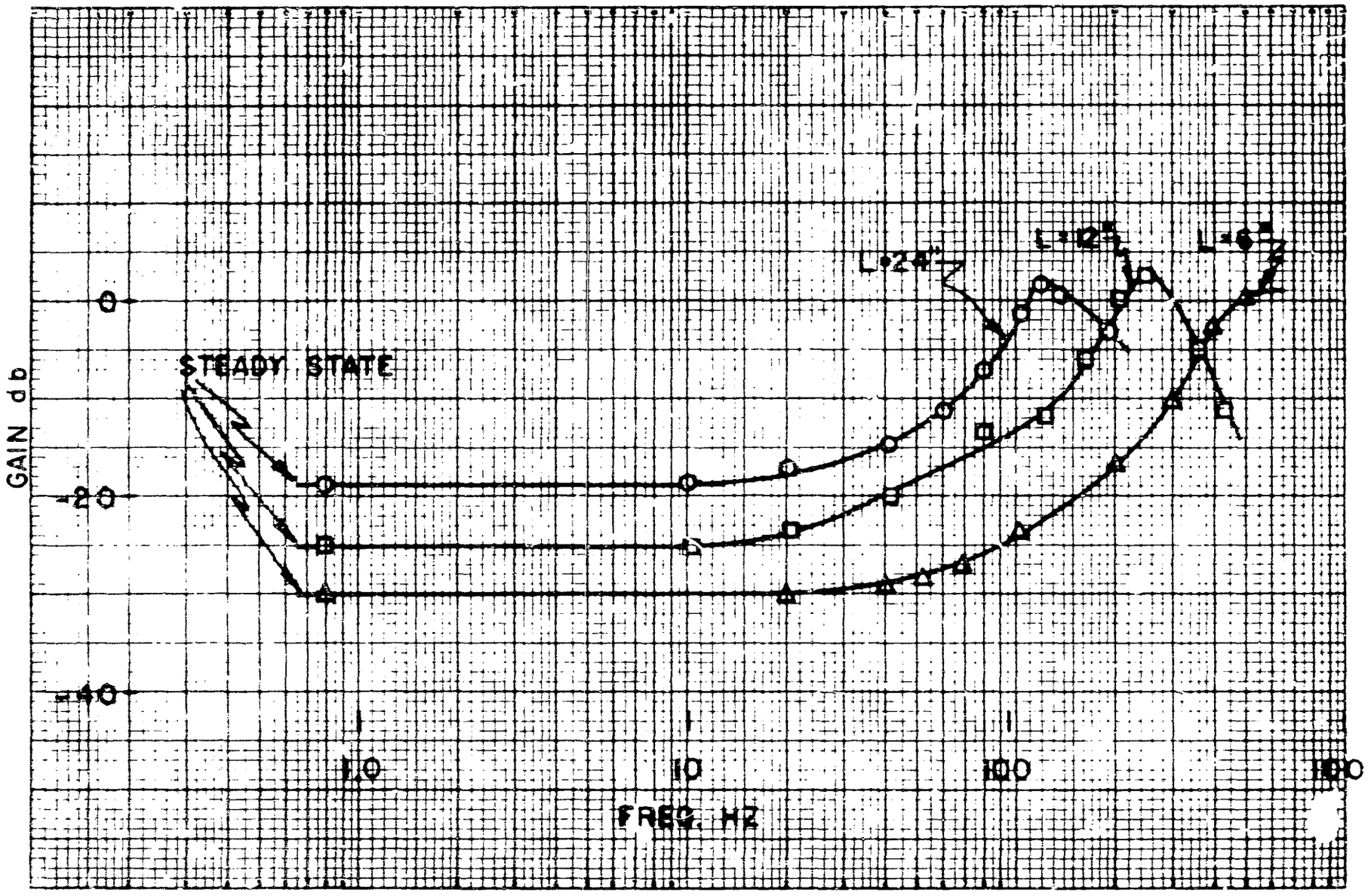


FIG.4.9 INDUCTIVE LEAD-LAG
(GAIN VS FREQ.)

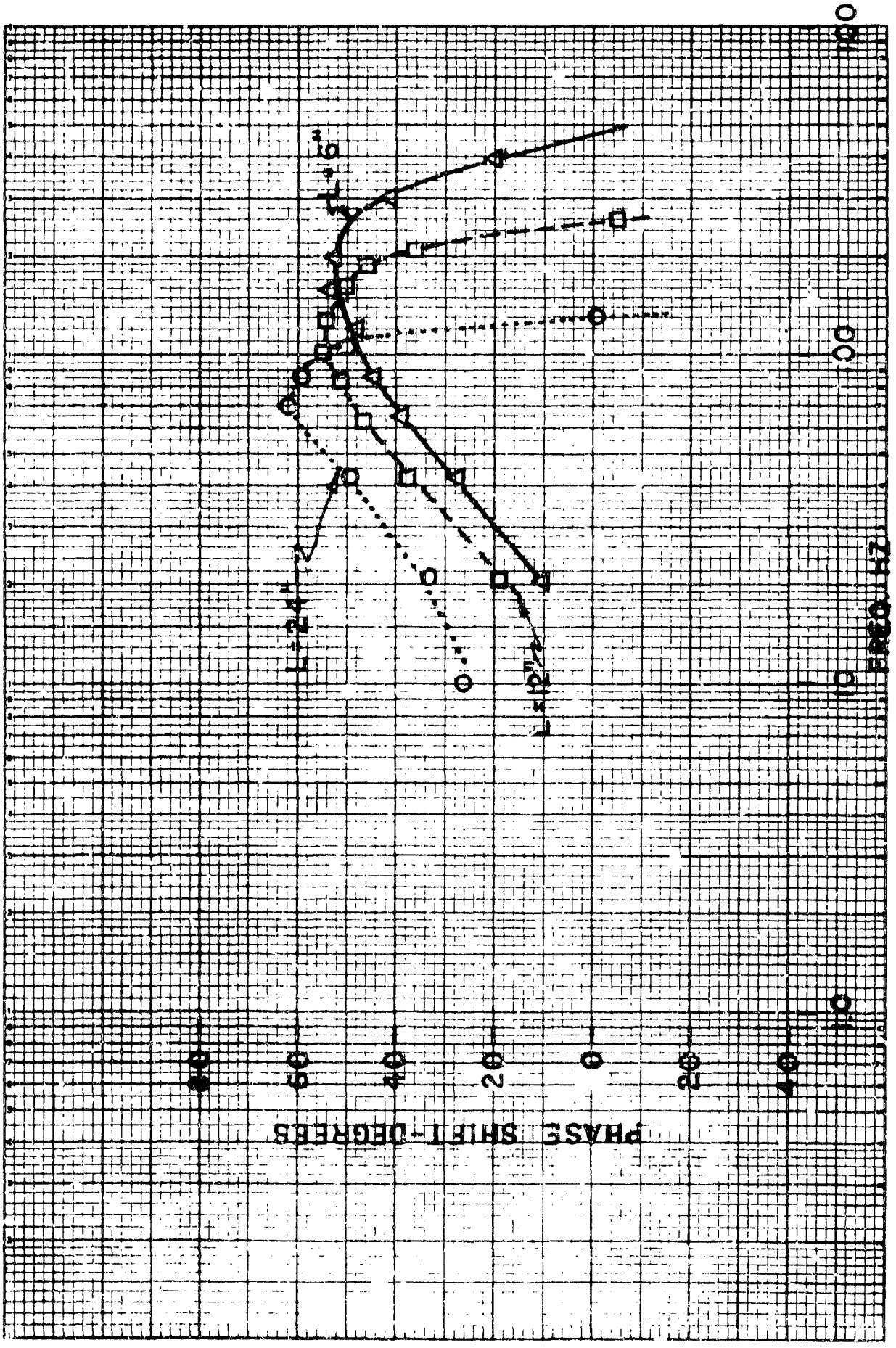


FIG. 4.10 INDUCTIVE LEAD-LAG
(PHASE VS FREQ.)

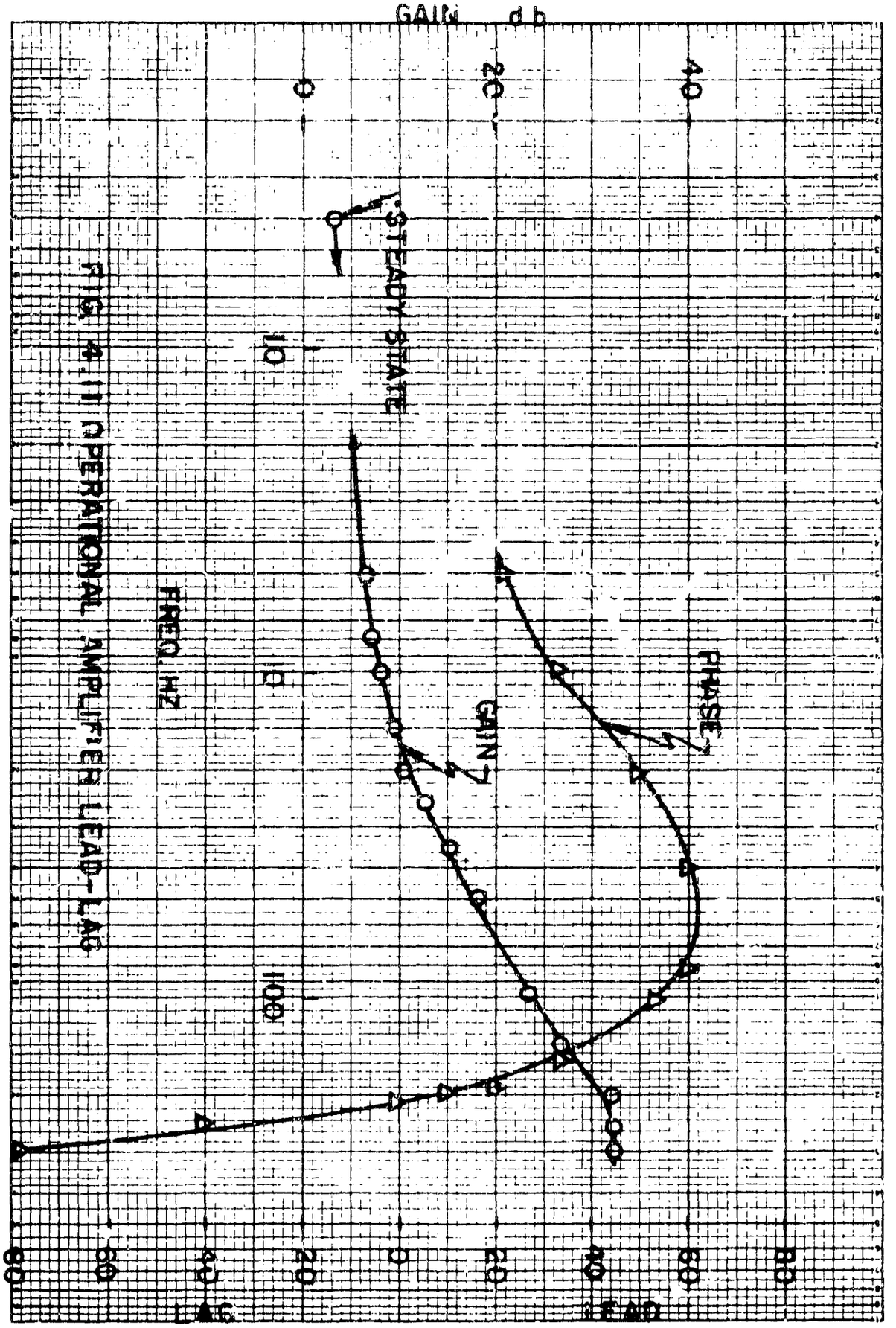


PHASE SHIFT — DEGREES

## 4.5 Base and Manifold

The main objective of the layout design is to achieve as short a signal path as possible (each 1 inch of length contributes $3^{o}$ phase lag @ 100 HZ) and to provide a stable base to attach the seismic mass and pick-off amplifiers. Provision must also be made for trimming the accelerometer. The general layout and assembly is shown in drawing 542C 00 and 422D565 in the appendix.

The signal path essentially doubles back on itself in going from the pick-off back to the nulling nozzle. The path length is slightly under 4 inches in the manifold assembly which results in a phase lag of $12^{o}$ at 100 HZ.

The only adjustment on the accelerometer which is critical is alignment of the pick-off amplifier and the jet pipe. A relative course adjustment is required along the insensitive axis. This adjustment effects only the gain of the loop and is done by placing shims between the manifold and the amplifier base. Correct shim height can be determined by visual inspection. The second adjustment trims out any biases in the accelerometer and should be made with the accelerometer operating closed loop. The accelerometer is mounted on a horizontal surface so that zero g's are applied to the mass. With a manometer on the accelerometer output the pick-off amplifier is moved along the sensitive axis until the output of the accelerometer is nulled. The pick-off amplifier is secured in this position.

Connections to the assembly consist of one pneumatic power supply line and two output lines.

## 5.0 TESTS

This section describes the tests which were made to determine the static and dynamic characteristics of the accelerometer.

### 5.1 Static Tests

The determination of scale factor, stability of scale factor, linearity and bias g's are the prime objectives of static tests on the accelerometer. These tests are made by varying the inclination angle of the sensitive axis relative to gravitational acceleration.

Figure 5.1 is a plot of accelerometer output vs. g for two values of supply pressure. A 25 percent increase in supply pressure results in a 3% increase in scale factor. The measured change is in close agreement with the predicted based on a loop gain of 10.

Scale factor vs. temperature was measured by setting a fixed inclination angle on the accelerometer and then varying temperature without disturbing the angle. The output was monitored to measure the pressure drop across each nulling nozzle as well as the differential pressure. A representative test result is shown in Figure 5.2. In general, the characteristics of the circuits changed as evidenced by the increase pressure drop across each nozzle as temperature increased. However, the differential pressure remained relatively constant. The expected change in scale factor is less than .5% over the temperature range tested. Test results show negligible changes with temperature.

Null shift vs. temperature was determined by setting the inclination angle for zero applied g and then varying the temperature. Results are shown in Figure 5.3. The pressure drop across each nozzle is plotted as well as the equivalent null shift. The equivalent g's were determined from the measurement of differential pressure and measured scale factor. The change in null is approximately .006g over the temperature range tested. This is well within the linearity and scale factor requirements.

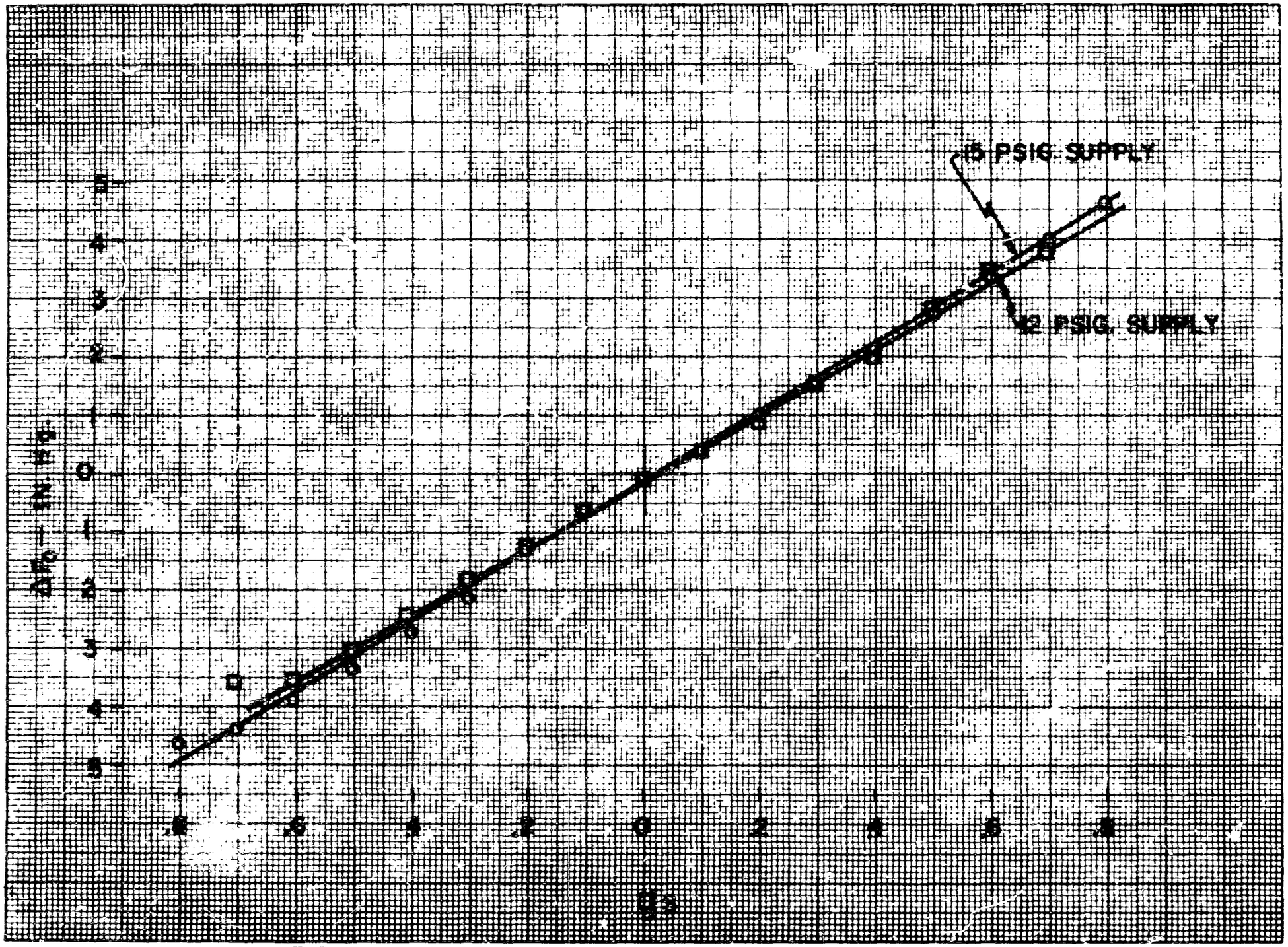


FIG. 5.1 CHANGE IN SCALE FACTOR VS SUPPLY

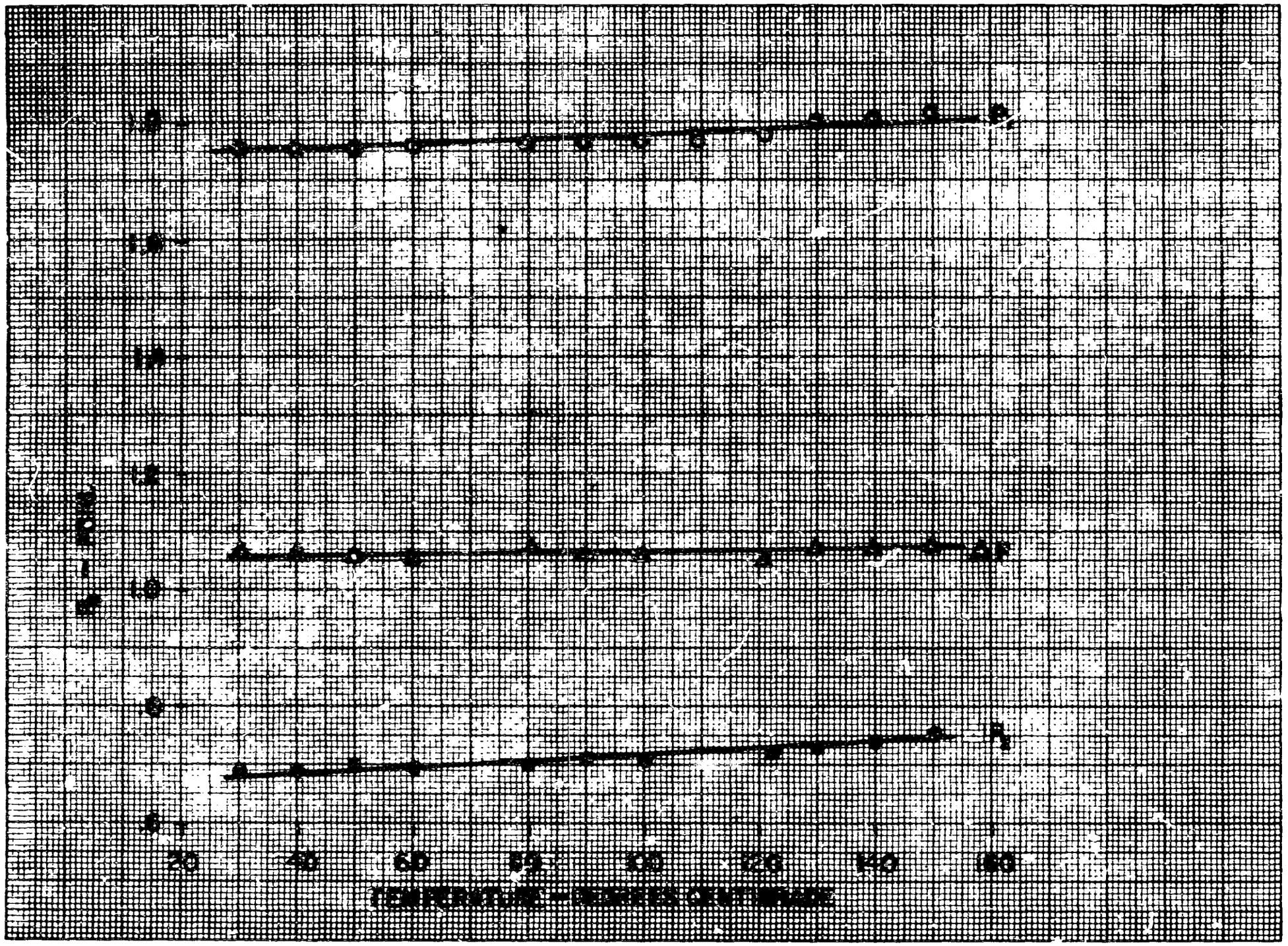


FIG. 5.2 OUTPUT CHANGE VS TEMPERATURE

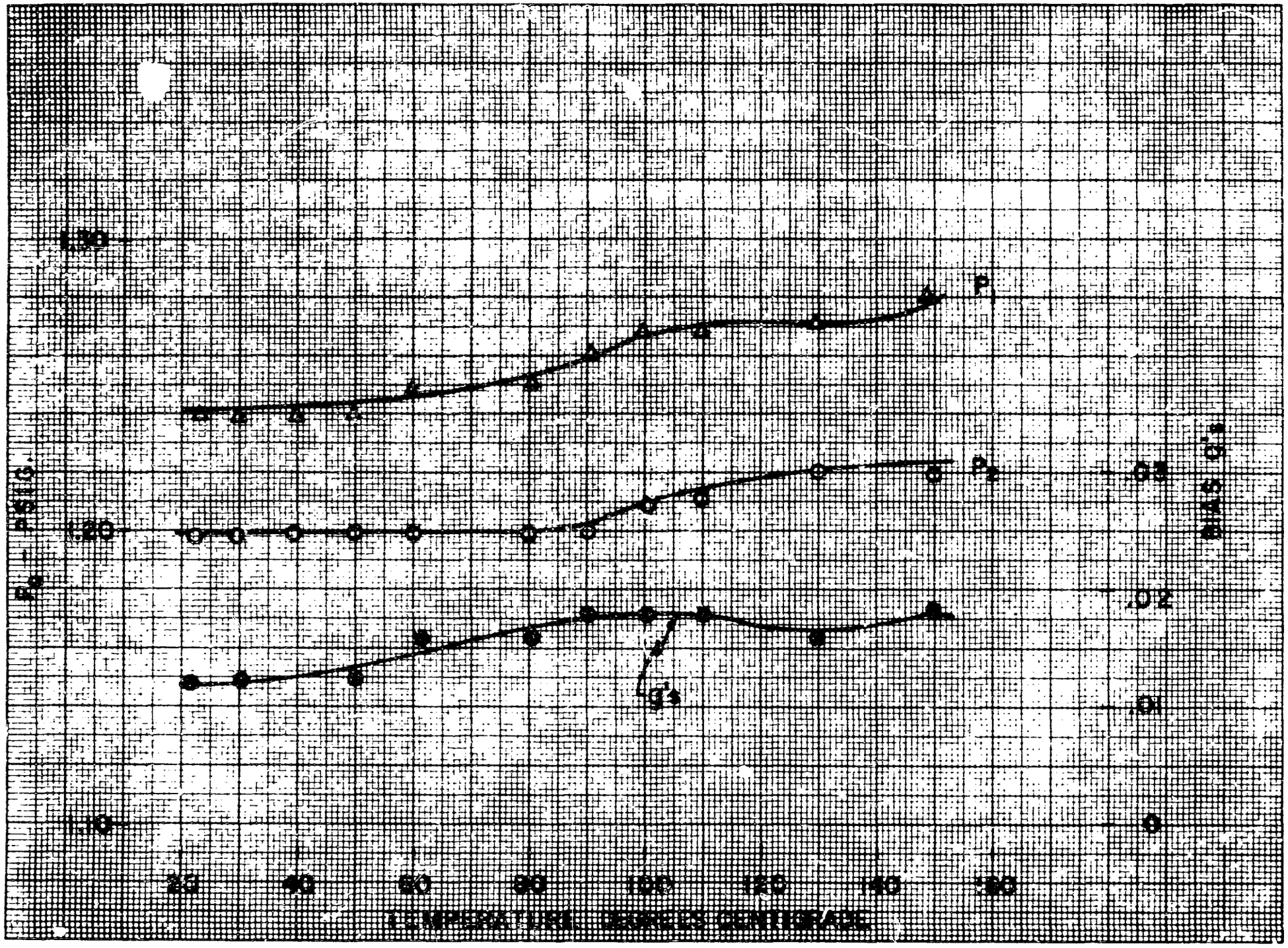


FIG. 5.3 NULL SHIFT VS TEMPERATURE

The RMS noise vs. bandwidth is shown in Figure 5.4. The noise is given in equivalent g's. Noise was measured directly across the nulling nozzles and passed through the indicated low pass filter. The noise is fairly well concentrated at the low end of the frequency spectrum as evidenced by the steep slope of noise vs. bandwidth at the low frequencies. In many applications noise will determine the minimum detectable g and is representative of the accelerometer threshold.

## 5.2 Dynamic Tests

Dynamic tests were performed to establish the accelerometer gain and phase characteristics vs. frequency. Both open and closed loop tests were performed.

Open loop tests were made by coupling the output of a pneumatic signal generator into the accelerometer nulling nozzles. The output amplifier was loaded with a dummy load simulating the nulling nozzles. The input pressure to the nulling nozzles was then compared to the output pressure across the dummy load. This method includes the dynamics of all components of the accelerometer.

Closed loop tests were performed by exciting the seismic mass with a signal generator coupled into a set of auxiliary nozzles. The input to the auxiliary nozzles was then compared to the output across the accelerometer nulling nozzles.

Closed loop test results were summarized in section 2. Data on response and phase lag is shown in Figure 2.6 and 2.7.

Open loop test results are plotted in Figures 5.5 to 5.7. Results in Figures 5.5 and 5.6 were obtained with a lead break frequency of 20HZ in the lead-lag operational amplifier. Open loop cross over is at 80 HZ. Preliminary test results as shown in Figure 5.5 exhibited a lightly damped resonance in the system at 220 HZ. The accelerometer was unstable and oscillated at that frequency when the loop was closed. The source of the resonance was found to be a secondary mode of oscillation on this flexure. The frequency of this mode is determined by the moment of inertia of the seismic mass about its center of mass and the

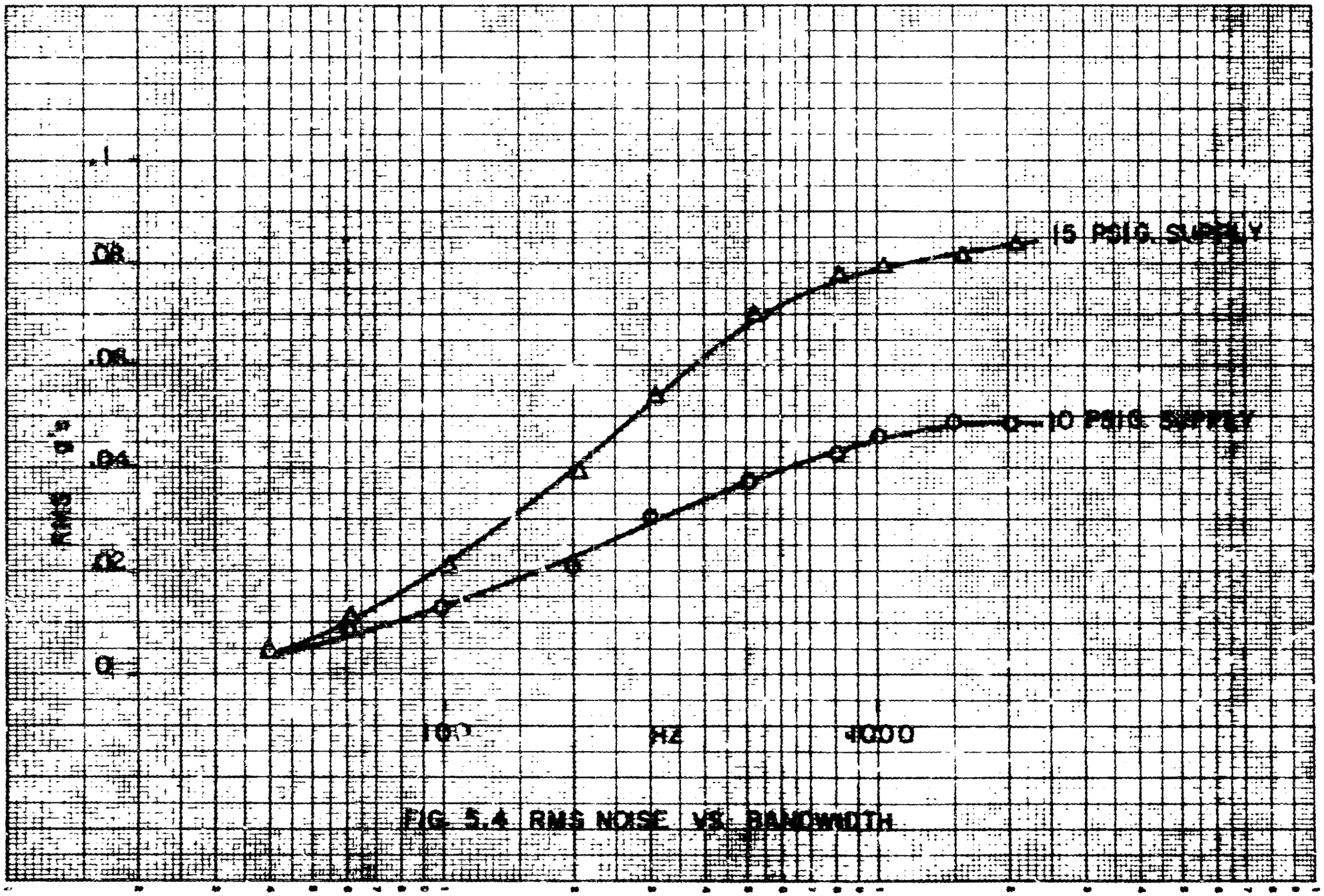


FIG. 5.4 RMS NOISE VS. BANDWIDTH

flexure spring gradient resisting the turning moment about the center of mass. This mode can be excited by any couple about the center of the mass, the couple is minimized when the axis of the nulling nozzles coincides with the center of mass. Figure 5.6 is a gain plot after adjusting the nulling nozzles to reduce the couple, so that stable closed loop operation can be obtained.

From Figures 5.5 and 5.6 it is evident that open loop phase lead drops off fairly rapidly above 80 HZ and, consequently, 80 HZ represents a realistic upper limit on system cross over. The range of this accelerometer was only $\pm$ .6g. Extension of the range requires an increase in proportional gain and a corresponding increase in system loop cross over. Unstable operation will be encountered with any significant increase in cross over. Moderate increases in range can be made if the lead break frequency is increased at the same time that the proportional gain is increased. This tends to lower the overall loop cross over - the loop cross-over tends to approach the minimum cross over indicated in section 3.1. Figure 5.7 is a plot of open loop gain and phase after modification to extend the range to $\pm$ .8g. The increase in range was made by compromising response and phase lag as evidenced by Figures 2.6 and 2.7.

Compliance with the design goals with respect to both range and response will require an integrator in the fluidic circuit.

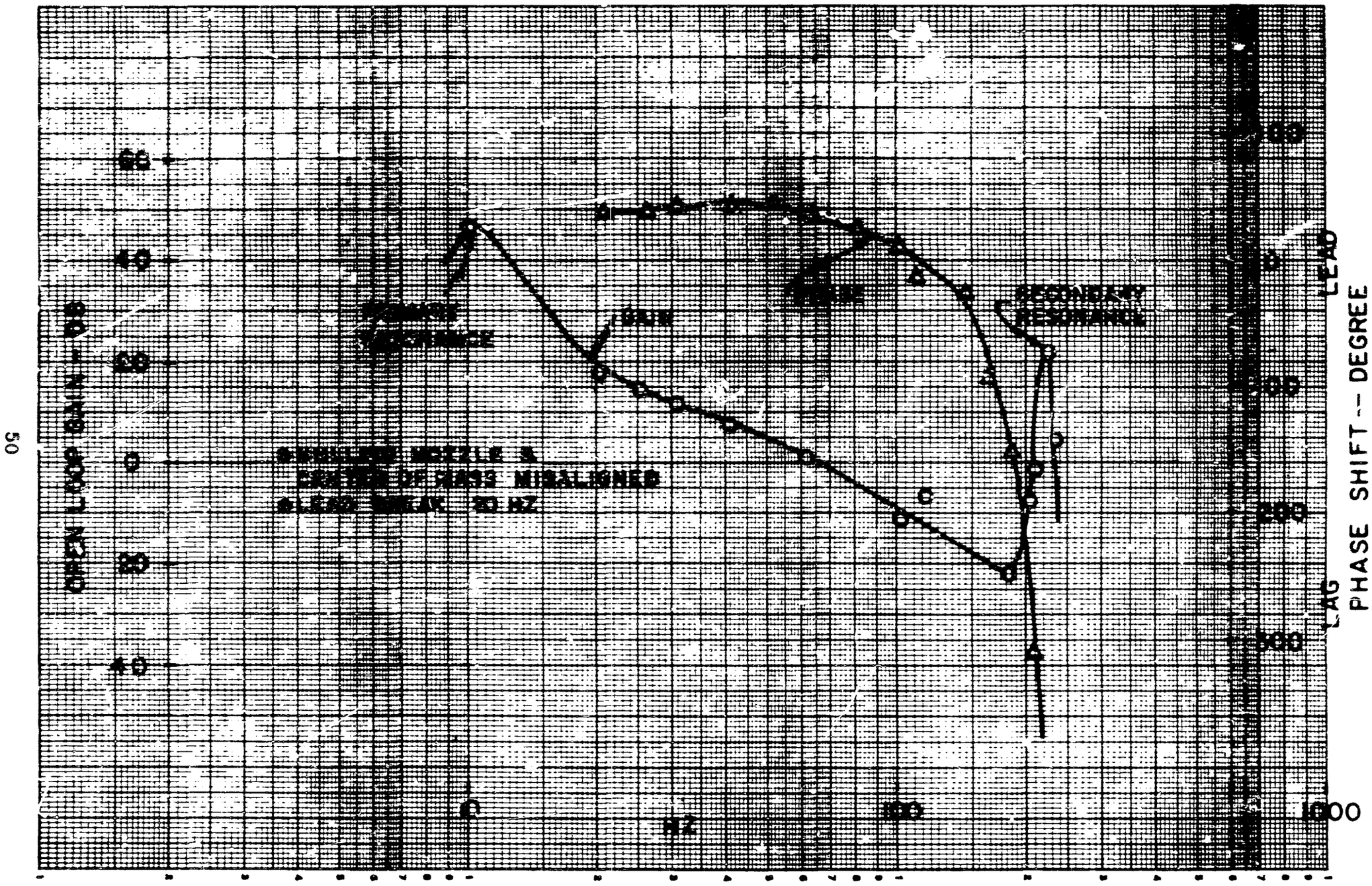


FIG. 5.5 OPEN LOOP GAIN & PHASE

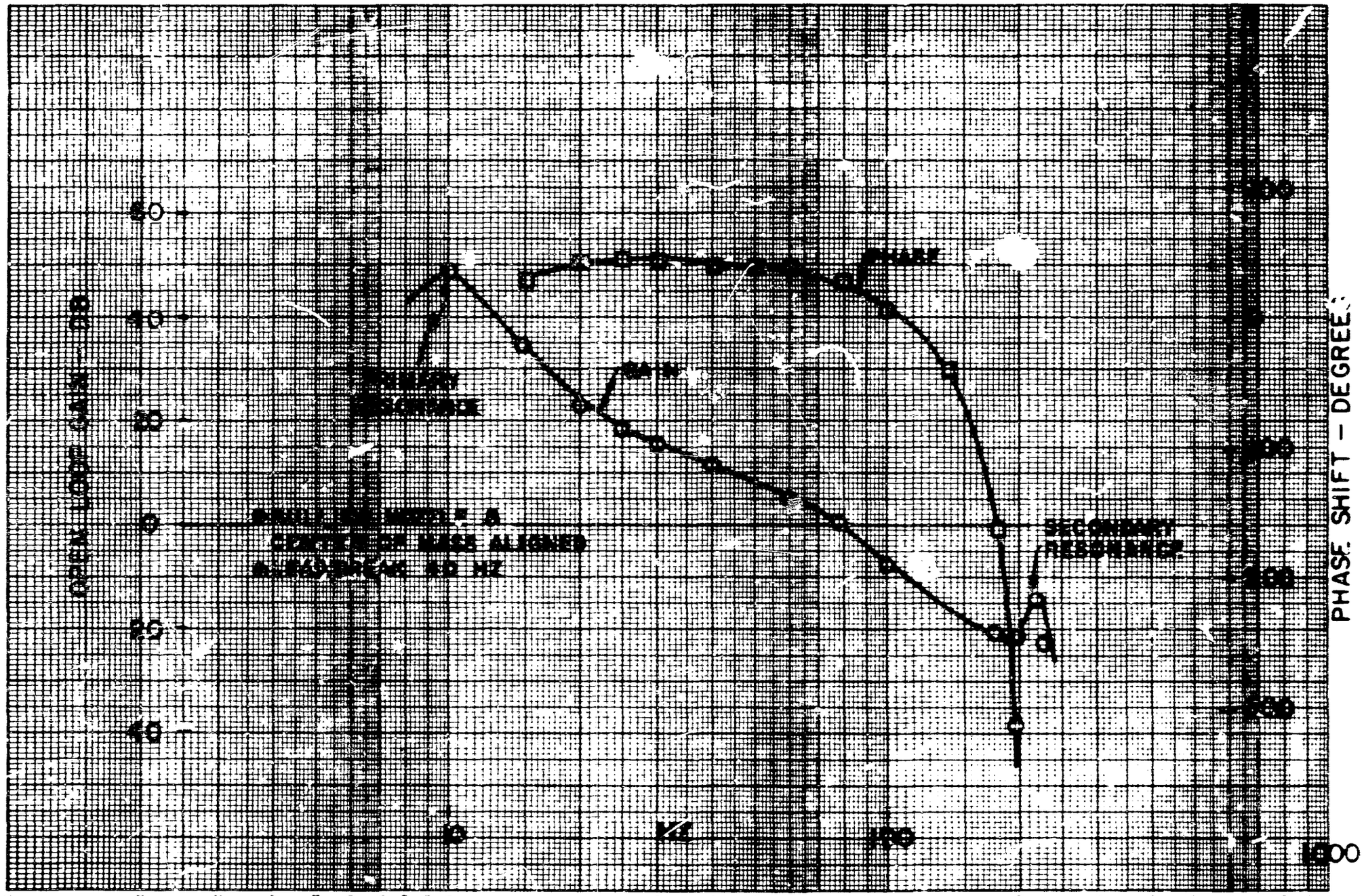


FIG. 5.6 OPEN LOOP GAIN & PHASE

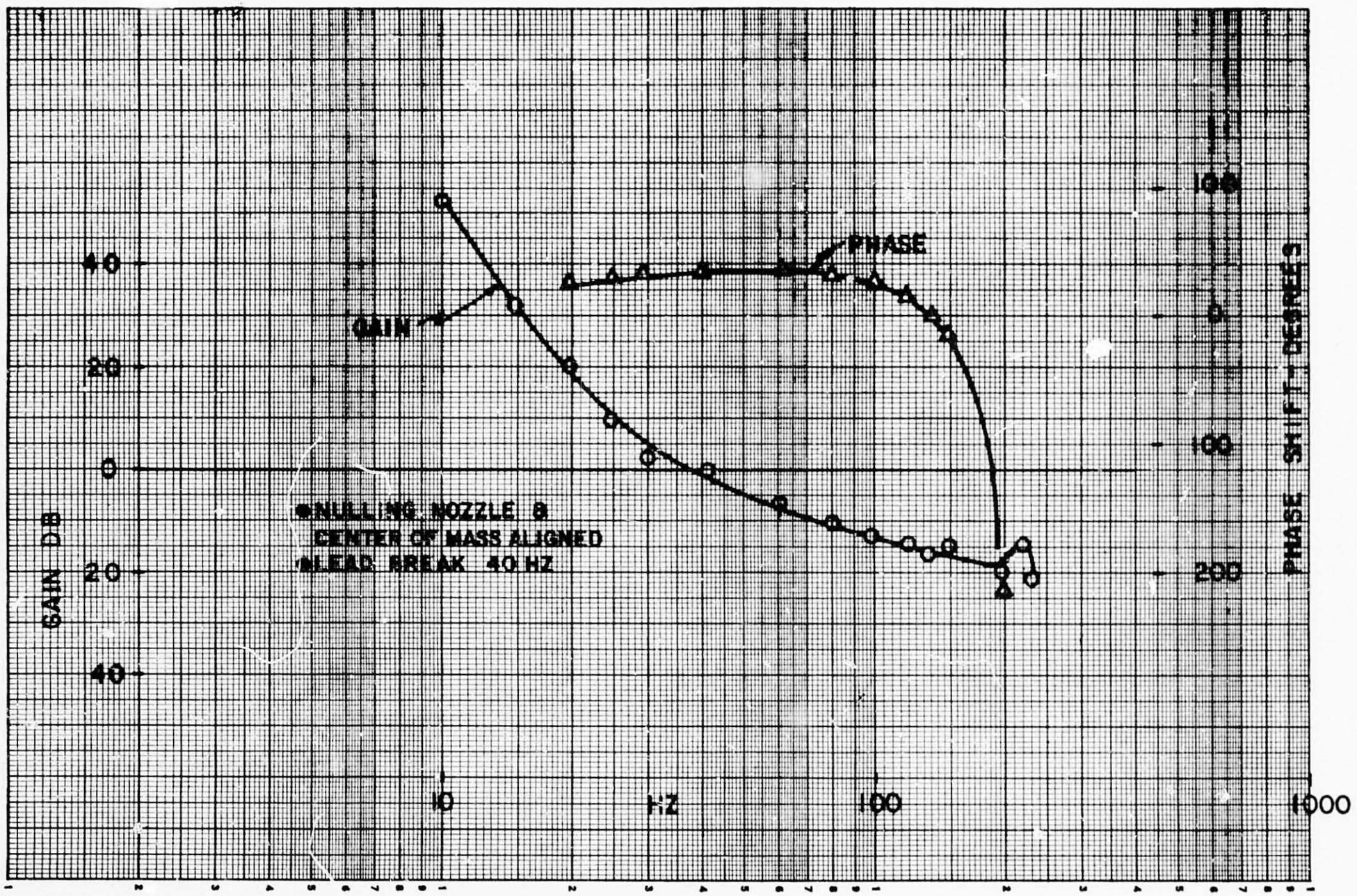


FIG. 5.7 OPEN LOOP GAIN & PHASE

# APPENDIX

## ACCELEROMETER DRAWINGS

| | |
|---|---|
| Assembly | 422 D 565 |
| Base and Manifold | 542 C 600 |
| Flexure | 542 C 601 |

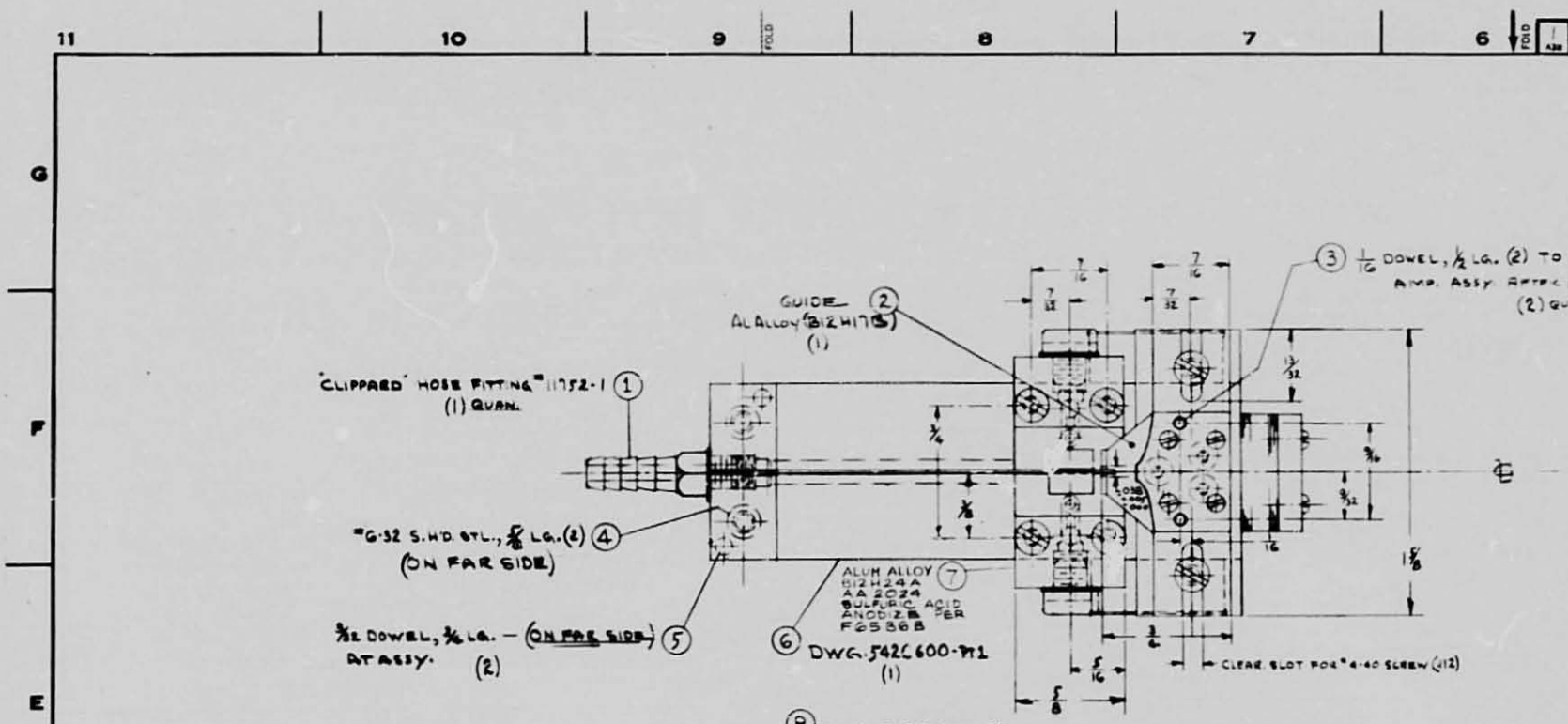


Foldout Frame 1

6 FOLD A 422D565 D 3270 4 FOLD 3 2 1

| REVISIONS | | | | |
|---|---|---|---|---|
| ZONE | LTR | DESCRIPTION | DATE | APPROVED |
| | | DIA., DEPTH, STYLE, & CANS - CHANGE FROM FOLDER TO SCREW (CANS) - MATERIAL CHANGE #1 - #11 | 10/19/67 | W. G. Lusher |

G F E D

EL, 1/2 LG. (2) TO SECURE PICK-OFF
MP. ASSY. REFR. ALIGNMENT.
(2) REQ'D.

W (112)

LG (4)

LH241) .091 THK.
E DRILLED
AL LAMINATION.

(12) ALIGNMENT SCREWS
#4-40 B.H.C. STL. 3/8 LG (2)

(3)

1/2

2)
RING (2)
PS PA
-7 SE
QUIVALENT

(13)
2)

.812 DIA.

(13)

RNISHED

"O" RING (2)
PARKER SEAL CO.
# S-136 S604-7
OR EQUIVALENT

CAN (2) —
HUDSON TOOL &
DIE PART
NO. HU-2270-STN. STL.

3/16 DEEP

40 R.HD. STL. 3/8 LG. (4)

| UNLESS OTHERWISE SPECIFIED DIMENSIONS ARE IN INCHES— TOLERANCES ON: | |
|---|---|
| 2-PLACE DECIMALS ± | ALL SURF |
| 3-PLACE DECIMALS ± .005 | |
| ANGLES ± | |
| FRACTIONS ± 1/32 | 125 |
| MATERIAL— | |

| SIGNATURES | DAY | MO | YR |
|---|---|---|---|
| DRAWN R. J. Burke | 21 | 11 | 67 |
| CHECKED | | | |
| ISSUED R. J. B | 1 | 12 | 67 |
| ENGRG | | | |
| MFG | | | |
| MATLS | | | |

GENERAL ELECTRIC
R&D CENTER DEPT LOC SCHDY.

NASA ACCELEROMETER

| SIZE | CODE IDENT NO. | |
|---|---|---|
| D | | 422D565 |
| SCALE 2X | | SHEET |

DIST TO

6 FOLD 5 4 FOLD 3 2 1

Fold out Frame 2

| SIZE | DRAWING NO. | REV |
|---|---|---|
| C | 542C600 | 7 |

**REVISIONS**

| ZONE | LTR | DESCRIPTION | DATE | APPROVED |
|---|---|---|---|---|
| DE/F DC/4 | 1 | ADDED TOLERANCES .043 ± .090 DIA HOLES CHANGED DIA. - ADDED .032 GROOVE - ADDED 6-32 HOLE - CHANGED DEPTH GROOVE MATERIAL | 2/9/68 | D.C. Fowler |

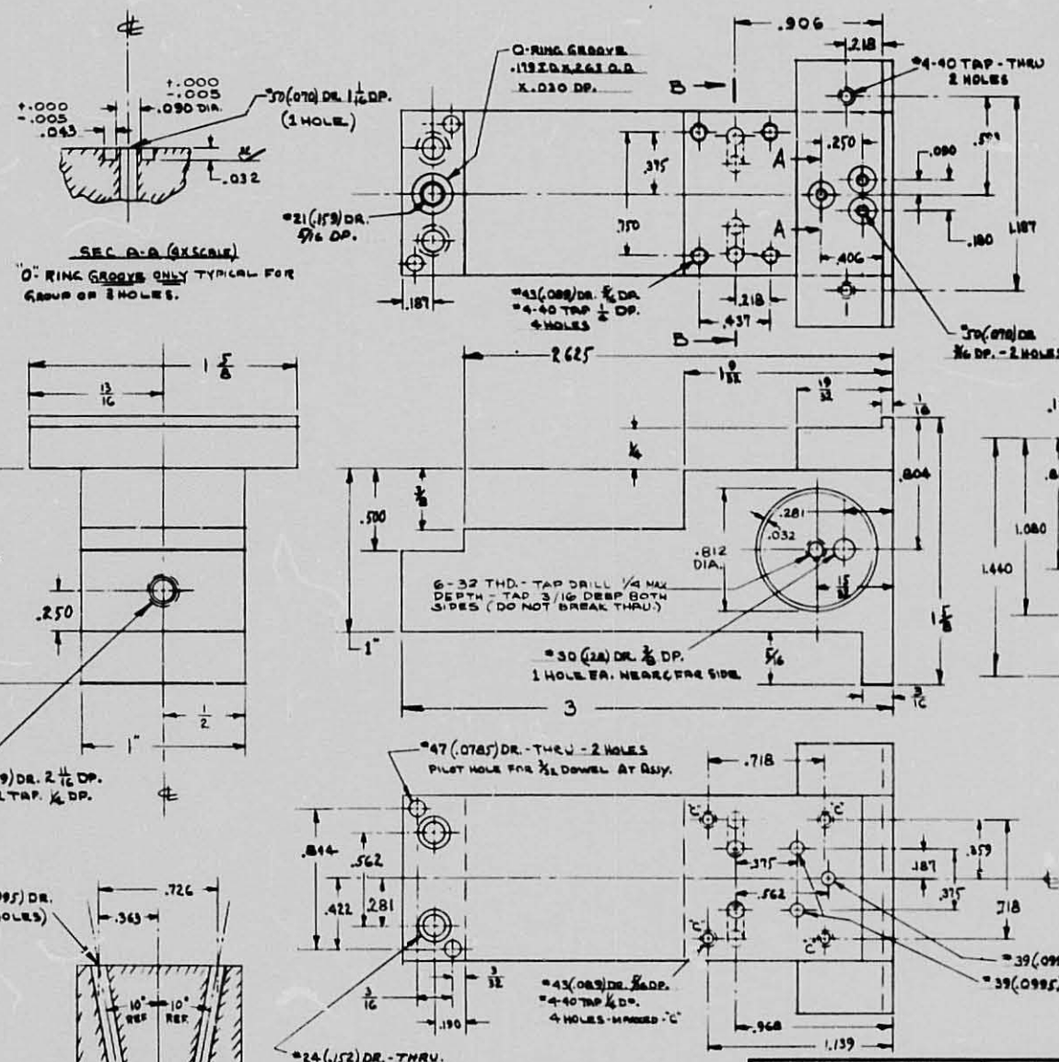


1

MATERIAL: ALUM ALLOY B2H24A
AA 2024
SULFURIC ACID ANODIZE
PER F65B6B

UNLESS OTHERWISE SPECIFIED DIMENSIONS ARE IN INCHES—
TOLERANCES ON:
2-PLACE DECIMALS ± ALL SURF
3-PLACE DECIMALS ± .005
ANGLES ± 1°
FRACTIONS ± 1/64
MATERIAL—

| SIGNATURES | DAY | MO | YR |
|---|---|---|---|
| DRAWN | 28 | 11 | 67 |
| CHECKED | | | |
| ISSUED | 1 | 12 | 67 |
| ENGRG | | | |
| MFG | | | |
| MATLS | | | |

GENERAL ELECTRIC
R&D CENTER DEPT LOC SCHDY

# MANIFOLD

PMR: NASA ACCELEROMETER R.C.P. DWG. 422D565

| SIZE | CODE IDENT NO. | 542C600 |
|---|---|---|
| C | | |

SCALE 2X SHEET

DIST TO

REV 1 542C600 SEC C

FN 903 F (4-67) PRINTED IN U.S.A.

| SIZE | | REV |
|---|---|---|
| C | 542C601 | |

REVISIONS

| ZONE | LTR | DESCRIPTION | DATE | APPROVED |
|---|---|---|---|---|
| | 1 | TITLE CHANGE - FROM VIBRATOR TO FLEXURE | 12/7/67 | |

CARE MUST BE TAKEN WITH THE PROCEDURE FOR BRAZING, SO THAT BRAZING MATERIAL DOES NOT WEAKEN S.S. TUBING AT THESE POINTS.
* SEE SUGGESTION FOR FEEDING BRAZE MATERIAL.

GOLD-COPPER BRAZE COMPLETE ASSY. THIS INTERFACE MUST BE LEAKTIGHT

* FEED BRAZE MATERIAL ALONG THIS SEAM

GOLD-COPPER BRAZE

(5) GAUGE 32 (.009 O.D. x .004 I.D.) S.S. HYPO. NEEDLE TUBING - 2 3/32 LG. USED AS SUPPORT ONLY

* FEED BRAZE MATERIAL AT THIS & OPPOSITE END.

END OF TUBE

APPROX. 1/8

1/32 x 45° CHAMF.

(6) GAUGE 26 (.018 O.D. x .008 I.D.) S.S. HYPO. NEEDLE TUBING - 2 3/32 LG. ORIFICE MUST BE CHECKED.

.281 .500 .562 1" REF.

#36 (.107) DR., 5/16 DP.
#6-32 TAP, 1/4 DP. - 2 HOLES

(4)

(G1)

PARTIAL VIEW "B" (8X SCALE)

SEC A-A (8X SCALE)

| UNLESS OTHERWISE SPECIFIED DIMENSIONS ARE IN INCHES— TOLERANCES ON: | |
|---|---|
| 2 PLACE DECIMALS ± | ALL SURF |
| 3 PLACE DECIMALS ± .005 | |
| ANGLES ± 1° | |
| FRACTIONS ± 1/64 | 63 |
| MATERIAL— B7A54A | |

| SIGNATURES | DAY | MO | YR |
|---|---|---|---|
| DRAWN | 30 | 11 | 67 |
| CHECKED | | | |
| ISSUED | 1 | 12 | 67 |
| ENGRG | | | |
| MFG | | | |
| QUALITY | | | |

GENERAL ELECTRIC
R&D CENTER DEPT LOC SCHDY

FLEXURE

F.M.F. NOISE ACCELEROMETER PROJ. DWG. 4220565

| SIZE | CODE IDENT NO. | |
|---|---|---|
| C | | 542C601 |

SCALE 2X SHEET

DIST TO

REV 1

SIZE C 542C601

FN 903-F (4-67)
PRINTED IN U.S.A.